Aurora B is required for programmed variations of cytokinesis during morphogenesis in the *C. elegans* embryo

Xiaofei Bai[1], Po-Yi Lee[3], Chin-Yi Chen[3], James R. Simmons[1], Benjamin Nebenfuehr[1,4], Diana Mitchell[1,5], Lindsey R. Klebanow[1,6], Nicholas Mattson[1,7], Christopher G. Sorensen Turpin[1], Bi-Chang Chen[2,3], Eric Betzig[2], Joshua N. Bembenek[1*]

[1] Department of Biochemistry, Cellular and Molecular Biology, University of Tennessee, Knoxville, Tennessee, United States of America.

[2]Janelia Research Campus, HHMI, Ashburn, Virginia, United States of America.

[3]Research Center for Applied Science, Academia Sinica, Taiwan.

[4]Current Address: NIDDK, NIH, Bethesda, MD, United States of America.

[5]Current Address: Biological Sciences, University of Idaho, Moscow, Idaho, United States of America.

[6]Current Address: Parker Hannefin Corporation, Macedonia, Ohio, United States of America

[7]Current Address: USFDA/CDER/OPQ/OBP/DBRRI, Silver Springs, MD, United States of America

* Corresponding Author:
Joshua N. Bembenek
1414 Cumberland Ave.
C211 Walters Life Sciences Building
Knoxville, TN 37996
(865)-974-4085
E-mail: bembenek@utk.edu

Abstract

While cytokinesis has been intensely studied, how it is executed during development is not well understood, despite a long-standing appreciation that various aspects of cytokinesis vary across cell and tissue types. To address this, we investigated cytokinesis during the invariant *C. elegans* embryo lineage and found several reproducibly altered parameters at different stages. During early divisions, furrow ingression asymmetry and midbody inheritance is consistent, suggesting specific regulation of these events. During morphogenesis, we find several unexpected alterations including migration of midbodies to the apical surface during epithelial polarization in different tissues. Aurora B kinase, which is essential for several aspects of cytokinesis, remains localized to the apical membrane after internalization of other midbody components. Inactivation of Aurora B causes cytokinesis failure, which disrupts polarization and tissue formation. Therefore, cytokinesis shows surprising diversity during development and is required during epithelial polarization to establish cellular architecture during morphogenesis.

Introduction

Generation of a multicellular organism requires that carefully orchestrated cell division is integrated properly into different developmental processes. Cell division is required not only to generate new cells that organize into tissues, but also to dictate the size, position and timing of daughter cells that are generated. Several aspects of cell division, including spindle orientation and division symmetry are well known instruments of developmental programs (Siller and Doe, 2009). Roles for cytokinesis in regulating developmental events are emerging, but are much less understood (Chen et al., 2013; Herszterg et al., 2014; Li, 2007). Using advanced live imaging, we sought to investigate cytokinesis in the well-defined divisions of the invariant *C. elegans* embryo lineage, which has been completely described (Sulston et al., 1983).

Cytokinesis is the final step of cell division and is normally a constitutive process during the exit from mitosis defined by discrete steps that occur during "C phase" (Canman et al., 2000; Oegema and Hyman, 2006). During cell division, signals from the anaphase spindle initiate ingression of the cleavage furrow (Bringmann and Hyman, 2005; Eggert et al., 2006), which constricts the plasma membrane onto the spindle midzone and leads to formation of the midbody. The midbody is a membrane channel between daughter cells containing microtubules and a defined organization of more than one hundred proteins that collaborate to execute abscission, the final separation of daughter cells (Green et al., 2012; Hu et al., 2012; Skop et al., 2004). Many of the proteins that contribute to midbody formation and function have roles in the formation of the central spindle and the contractile ring (El Amine et al., 2013). In addition, vesicles are delivered to the midbody that contribute lipids as well as regulators of abscission (Schiel et al., 2013). Subsequently, the ESCRT machinery assembles, microtubules are cleared and membrane scission occurs (Guizetti et al., 2011; Schiel et al., 2011). Aurora B kinase (AIR-2 in *C. elegans*) is essential for cytokinesis, acting on a number of targets although its precise mechanism is not fully elucidated. Aurora B also prevents completion of abscission in response to developmental or cell cycle cues partly by regulating the ESCRT machinery (Carlton et al., 2012; Carmena et al., 2015; Mathieu et al., 2013; Norden et al., 2006; Steigemann et al., 2009). How abscission is regulated in different developmental contexts has not been thoroughly investigated. In general, while mechanistic details of cytokinesis are being elucidated, it is generally assumed that these events occur through a standard, well-defined series of ordered events.

Exceptions to such a clear linear view of cytokinetic events have long been known, but are considered to be specialized cases. The most extreme examples are cells that do not complete cytokinesis altogether and become polyploid, such as liver or intestinal cells (Amini et al., 2015; Fox and Duronio, 2013; Hedgecock and White, 1985; Lacroix and Maddox, 2012). Another well-known example is found in several systems where germ cells do not complete abscission and remain connected through ring canals, which can allow flow of cytoplasm into germ cells (Greenbaum et al., 2007; Haglund et al., 2011; Hime et al., 1996; Maddox et al., 2005). Delayed abscission has also been observed in other cell types to keep daughter cells connected (McLean and Cooley, 2013; Zenker et al., 2017). Other variations of cytokinesis include cleavage furrow re-positioning during anaphase to change the size and fate of daughter cells (Ou et al., 2010). The symmetry of furrow ingression is important in established epithelial tissue where the furrow constricts toward the apical side of the cell and must occur while appropriate cellular contacts are preserved (Herszterg et al., 2014). In zebrafish neuroepithelial divisions, asymmetrical furrowing positions the midbody at the apical domain, which is inherited by the differentiating daughter (Paolini et al., 2015). Therefore, there are a number of ways the standard pattern of cytokinesis can be altered and more investigation is required to understand the functional purpose of these changes and how they are achieved.

Recent studies of abscission have sparked renewed interest in the midbody, which has led to insights into other functions it has beyond abscission (Chen et al., 2013). Recent evidence indicates that the midbody is cut off from each of the daughter cells that give rise to it (Crowell et al., 2014; Konig et al., 2017). The midbody may then be engulfed by either cell or persist extracellularly, which can depend on cell type (Ettinger et al., 2011; Salzmann et al., 2014). The midbody can also travel to non-parent cells, suggesting that it may carry or transport signals between cells (Crowell et al., 2014). The midbody is reproducibly inherited in *Drosophila* germline stem cells, but does not always end up in the stem cell (Salzmann et al., 2014). In dividing neuroepithelial cells, a stem cell marker is concentrated at the midbody and released into the lumen of the neural tube, which might provide signals during neuronal development (Dubreuil et al., 2007). This has led to the hypothesis that the midbody provides cues that regulate cell fate, although a detailed mechanistic understanding of this has not been elucidated.

111 A more clearly defined function for the midbody has been uncovered in cells
112 that undergo polarization events after the completion of cytokinesis. For example,
113 Madin-Darby canine kidney (MDCK) cells can establish apical basal polarity and
114 organize into a simple epithelial lumen structure (Reinsch and Karsenti, 1994). Apical
115 membrane markers are first delivered to the midbody during cytokinesis, establishing
116 an apical membrane at the interface between the first two daughter cells (Schluter et
117 al., 2009). Proper abscission and midbody positioning is required, in addition to
118 proper spindle orientation, for MDCK lumen formation (Lujan et al., 2016; Reinsch
119 and Karsenti, 1994). Polarized trafficking during cytokinesis has been shown to
120 promote lumen formation in other systems as well (Wang et al., 2014b). Abscission is
121 also delayed in acentrosomal blastomeres of the early mouse embryo to generate a
122 midzone-derived microtubule organizing center that directs delivery of apical
123 membrane markers to the plasma membrane (Zenker et al., 2017). The midbody
124 becomes the apical process in chick neuronal progenitors (Wilcock et al., 2007) and
125 defines the site of polarization for dendrite extension in *D. melanogaster* neurons
126 (Pollarolo et al., 2011). The midbody is also a polarizing cue in the *C. elegans* embryo
127 during the establishment of dorsoventral axis formation (Singh and Pohl, 2014;
128 Waddle et al., 1994). In addition, the midbody can play a role in cilium formation
129 (Bernabe-Rubio et al., 2016). Further effort is required to understand how cytokinesis
130 and the midbody regulate pattern formation in tissues.
131 We sought to better understand how different aspects of cytokinesis are
132 regulated during development by taking advantage of the well characterized invariant
133 *C. elegans* embryonic lineage. We investigated furrow symmetry, central spindle
134 dynamics, abscission timing and midbody inheritance. We find that cytokinesis
135 follows a lineage specific pattern and that furrow symmetry and midbody inheritance
136 is highly reproducible. During morphogenesis, abscission is delayed and the midbody
137 forms in the middle of the cell and migrates to the apical membrane in the developing
138 digestive and sensory tissues in *C. elegans*, which is a novel behavior. Unlike typical
139 cytokinesis events, different midbody components have different fates in different
140 tissues. Notably, Aurora B kinase remains localized to several apical surfaces after
141 internalization of other ring components. Inactivation of temperature-sensitive Aurora
142 B mutants causes sporadic cytokinesis defects that disrupt apical polarization of
143 microtubules and adhesion. Cytokinesis mutants also have disrupted tissue
144 organization, indicating an important role for specialized cytokinesis during

145 morphogenesis. Together, our results suggest that Aurora B kinase has a novel
146 function at the apical surface after cytokinesis during epithelial polarization and that
147 modified implementation of cytokinesis is critical for proper cellular organization
148 during animal development.

149 **Results**

150 **Cytokinesis in the first two mitotic divisions: asymmetric midbody inheritance**

151 We sought to systematically examine cytokinesis using lattice light sheet and
152 spinning disc confocal microscopy during the stereotypical divisions of the *C. elegans*
153 embryo, which has been extensively studied primarily in the first cell division due to
154 its size and ease of access. The first mitotic division of the P0 cell generates the larger
155 anterior daughter AB and the posterior daughter P1 (Fig. 1 A). We observed different
156 components that allow us to evaluate specific aspects of the cytokinetic apparatus
157 including the central spindle, the cytokinetic furrow and the midbody. We also chose
158 midbody markers that localize to the flank and ring sub-structures of the midbody
159 (Green et al., 2012). To observe the midbody flank region, we imaged Aurora B
160 kinase (AIR-2), microtubules, and the membrane trafficking regulator RAB-11 (Fig. 1,
161 3, and Video S1). We also imaged midbody ring markers including the non-muscle
162 myosin NMY-2, which also labels the contractile ring, and the centralspindlin
163 component ZEN-4 (Fig. 1 G-P and Video S1). While the first mitotic furrow shows
164 some variable asymmetry as previously reported (Maddox et al., 2007), the midbody
165 forms in a relatively central position between daughter cells (Fig. 1 B-C, G-H and L-
166 M). AIR-2::GFP, endogenous AIR-2 staining and tubulin show the expected pattern
167 of localization on the central spindle and midbody as expected (Fig. 1 B-C, Fig. S1 A-
168 D, Fig. 3 A-B and Video S1). The midbody from the first mitotic division is always
169 inherited by the P1 daughter cell (Fig. 1 A). The midbody microtubule signal
170 diminishes within 8 minutes after furrowing onset, which is a general indicator of
171 abscission timing (Fig. 3 B, I) (Green et al., 2013; Konig et al., 2017). AIR-2 is lost
172 from the flank over time but can be observed on the midbody remnant even after it is
173 internalized into P1 (Fig. 1 D-E and Video S1). Additionally, each of the ring
174 components behaves similarly to AIR-2, as expected (Fig. 1 I-J and N-O). Therefore,
175 AIR-2 and other ring components remain co-localized on the midbody throughout the
176 final stages of cytokinesis and are reproducibly internalized by the P1 daughter cell,
177 as previously observed (Bembenek et al., 2013; Ou et al., 2014; Singh and Pohl,
178 2014).

179 During the second round of division, we observed substantial, reproducible
180 changes in the pattern of cytokinesis, beginning with furrow symmetry. During the
181 AB daughter cell division, which gives rise to ABa and ABp, the furrow ingressed

182 from the outer surface until it reached the opposite plasma membrane in contact with
183 EMS (Fig. 1 D-E, I-J, N-O). We calculated a symmetry parameter using the ratio of
184 furrow ingression distance from each side of the furrow at completion (Maddox et al.,
185 2007). On average, the furrow symmetry parameter is 1.7 in the first division, while
186 the AB furrow is 21.6 and the P1 furrow is 16.1, indicating highly asymmetric
187 furrows in the second divisions (Fig. 1 V, X). The central spindle is swept from the
188 middle of the AB cell into contact with EMS during furrow ingression (Fig. 1 E,
189 Video S1). AIR-2 localizes to the central spindle, then the midbody flank and remains
190 associated with the midbody remnant after it is engulfed (Fig. 1 D-F, S-U and Video
191 S1). NMY-2 and ZEN-4 also follow the expected pattern during cytokinesis and
192 appear on the midbody that forms in contact with EMS (Fig. 1 I-J, N-O and Video S1).
193 RAB-11::GFP accumulates briefly prior to abscission in both the first and second
194 rounds of division and is not observed on the midbody afterward (Figure 1 Q-U), as
195 shown previously (Ai et al., 2009; Bai and Bembenek, 2017; Bembenek et al., 2010).
196 Therefore, all midbody markers examined behave as expected during the first two
197 divisions.
198 Our examinations confirmed the unusual and consistent pattern of midbody
199 inheritance after the AB division. The midbody from the AB cell division that forms
200 in contact with EMS after highly asymmetric furrowing is invariably engulfed by
201 EMS instead of either of the AB daughter cells (Fig. 1 F, K, P, U, Fig S1 D and Video
202 S1). Further, the midbody from the P0 division is also always inherited by EMS.
203 Microtubules in the midbody flank disappear within 8 minutes after furrowing in both
204 AB and P1 cell divisions, indicative of relatively fast abscission at this stage (Fig. 3
205 C-D and I). This analysis confirms expected patterns of midbody regulation and
206 midbody protein dynamics during the early embryonic divisions. These data reveal
207 reproducible furrow ingression symmetry and midbody inheritance, which likely
208 involve multiple mechanisms operating during cytokinesis in order to achieve this
209 highly reproducible pattern.
210
211 **Aurora B localizes to the apical membrane after midbody migration and**
212 **internalization in E8-E16 gut cytokinesis**
213 We next performed a similar detailed analysis of cytokinesis on three
214 developing tissues in morphogenesis, which revealed several novel patterns of
215 cytokinesis. During morphogenesis, cells undergo terminal divisions and start to form

216 tissues by polarizing and changing shape. The intestine is a well characterized
217 epithelial tube derived from the E blastomere that undergoes five embryonic divisions
218 (Leung et al., 1999). The E8 to E16 division occurs around 280 minutes after the first
219 cleavage, after which cells undergo a mesenchyme to epithelial transition involving
220 epithelial polarization and subsequently organize into a tube (Leung et al., 1999). Our
221 observations demonstrate that these cells are performing a highly modified
222 cytokinesis as they undergo polarization, which to our knowledge has not been
223 previously reported (Fig. 2 A). The E8 cells undergo symmetrical furrowing to
224 produce a centrally placed midbody (Fig. 2 B, E, I, Fig. S2 A and Video S2-4) with a
225 1.0 symmetry parameter (Fig 1 W, X), in contrast with the highly asymmetric furrow
226 and displaced midbody location during the AB cell division. Therefore, the E8-E16
227 division appears largely routine up until the point of midbody formation.
228 After midbody formation, there are several changes to the pattern of cytokinesis,
229 which occur during epithelial polarization. Using lattice light sheet imaging, we
230 observe that centrally located midbodies from both left and right daughter cell
231 divisions (Ealp, Earp, Epla and Epra) migrate across the width of the cell to the
232 nascent apical surface at the midline, which completes 30 minutes after furrow
233 ingression (Fig. 2 B-D and Video S2). The midbody flank region elongates during the
234 migration process and the flank microtubules persist for over 25 minutes on average
235 from furrow ingression to when they join other microtubules at the apical midline and
236 can no longer be distinguished, which is three times longer than the early divisions
237 (Fig. 3 F, H-I). AIR-2::GFP localizes along the extended length of the spindle
238 midzone microtubules as they move to the apical midline instead of becoming
239 confined to the midbody remnant as observed in early divisions (Fig. 2 E-H, M, and
240 Video S2-4). The ratio of the length of this midbody flank relative to the cell at the
241 greatest length is 0.47 (average 4.6 μm / 9.8 μm) in the intestinal cell division, which
242 is more than twice that of the early two cell divisions 0.17 (average 9.3 μm/ 53.4 μm)
243 in P0 and 0.17 (average 7.7 μm/ 44.3 μm) in AB (Fig. 2 P-Q). The ring markers ZEN-
244 4 and NMY-2 are quickly internalized (553±140 seconds and 545±179 seconds,
245 respectively) after the midbody reaches the apical midline (Fig. 2 I-L, N-O and Video
246 S3). Collectively, these data indicate that abscission occurs after migration of the
247 midbody to the apical midline. Therefore, E8 cells undergo a programmed apical
248 midbody migration event instead of having an asymmetrical furrow lead to the
249 formation of an apically localized midbody, as observed in the AB cell division and

250 epithelial cells in other systems. To our knowledge this is the first observation of
251 collective midbody migration and may represent a new stage of cytokinesis.
252 In addition to this midbody migration event, we observed a novel behavior of
253 AIR-2 during E8-E16 cytokinesis. In contrast to the midbody ring components, AIR-2
254 remains localized at the apical midline well after the time that ring components are
255 internalized and polarization is complete (Fig. 2 D, G, H, M and Video S2-4), co-
256 localizing with the apical polarity marker PAR-6 (Fig S2 F-H). Endogenous AIR-2
257 can also be observed at the apical midline by immunofluorescence (Fig. S1 E-G). The
258 gut apical surface recruits pericentriolar material donated by the centrosome during
259 E16 polarization (Feldman and Priess, 2012; Yang and Feldman, 2015). We observed
260 that γ-tubulin::GFP moves to the apical surface at the same time as AIR-2::GFP (Fig.
261 S2 I). High temporal resolution single plane confocal imaging tracking individual
262 midbody dynamics confirm the elongated AIR-2::GFP flank localization and
263 persistence at the apical midline compared to the rapid internalization of ZEN-4::GFP
264 after the migration event (Fig. 2 M-N and Video S4). For comparison, we imaged the
265 first three E cell divisions and found symmetric furrowing (Fig. 1X), rapid abscission
266 timing (Fig. 3I) and that midbody behavior was similar to the early embryo divisions
267 with no exaggerated alterations (Fig. S3). Therefore, different midbody components
268 have different fates at the end of cytokinesis specifically in the E8-E16 intestinal
269 divisions during epithelial polarization, with ring markers being internalized while
270 AIR-2 remains at the apical surface. To our knowledge, this is the first report of AIR-
271 2 localization remaining at the plasma membrane after abscission.
272 In other lumen forming systems, such as MDCK cells, RAB-11 vesicle
273 trafficking during cytokinesis transports apical membrane components to the midbody
274 to establish the apical membrane (Schluter et al., 2009). In *C. elegans*, RAB-11
275 endosomes control trafficking at the apical surface of the intestine throughout the life
276 of the animal (Sato et al., 2014). We imaged RAB-11 during the E8-E16 division to
277 examine when apical localization occurs. RAB-11::mCherry colocalizes with AIR-
278 2::GFP once the midbody is formed and migrates to the apical surface with the
279 midbody (Fig. S2 J-L). RAB-11::mCherry is also localized at spindle poles, as in
280 other mitotic cells (Albertson et al., 2005), which also migrate to the apical surface
281 (Feldman and Priess, 2012). Similar to AIR-2, RAB-11 remains localized to the apical
282 surface well after cytokinesis is complete and remains at this position throughout the
283 life of the animal (Fig. S2 L). These observations indicate that the apical localization

284 of RAB-11 is established during cytokinesis in the E8-E16 division, which may
285 contribute to formation of the apical surface during intestinal epithelial polarization.
286 The anterior and posterior pair of E16 cells (Ealaa, Earaa, Eplpp and Eprpp)
287 undergo one last embryonic division to achieve the E20 intestine stage. In the four
288 central E8 cells that do not divide again, the midbody migrates to the midline at E8-
289 E16 as described above. However, the midbodies from the other four E8 cells (Eala,
290 Eara, Eplp and Eprp), which undergo another division, migrate toward the midline but
291 the AIR-2 signal diminishes (Fig. S2 E). During the final E16-E20 divisions, the
292 midbodies of Ealaa, Earaa, Eplpp and Eprpp undergo apical migration after
293 symmetrical furrowing (Fig. S2 M-O and Video S5). Therefore, the midbody
294 migration event in the intestine does not happen only during the polarization event
295 that occurs during E8-E16, suggesting that it is specifically programmed to occur
296 during the terminal embryonic divisions. Post-embryonic divisions in the intestine at
297 L1 lethargus involve nuclear but not cytoplasmic divisions leading to the formation of
298 binucleate cells that subsequently undergo multiple rounds of endoreduplication to
299 become highly polyploid (Hedgecock and White, 1985). Therefore, cytokinesis in the
300 intestinal lineage undergoes distinct regulatory phases at different stages of
301 development.
302
303 **Aurora B Kinase is required for normal E8-E16 cytokinesis and proper**
304 **epithelial polarization**
305 Given the pattern of cytokinesis during the E8-E16 division and the localization
306 of AIR-2::GFP to apical structures, we sought to investigate Aurora B function at this
307 stage of development. We first asked if cytokinesis is essential for the final stages of
308 embryonic development since it is possible that morphogenesis could occur despite
309 the presence of binucleate cells. To bypass the essential function of cytokinetic
310 regulators during the early embryonic cell divisions, we inactivated temperature
311 sensitive (ts) mutants after isolation of two-cell embryos at the permissive
312 temperature (15 °C) and shifted them to non-permissive temperature (26 °C) at
313 different embryo stages until they hatched. The *air-2(or207)* embryos have only 53.6%
314 (37/69) hatching even when left at 15 °C through hatching, indicating that this mutant
315 is sick even at permissive temperature, while wild-type N2, *zen-4(or153)* and *spd-*
316 *1(oj5)* embryos are 100% viable when kept at 15 °C (Table 1). Embryos shifted to
317 26 °C after 4.5 hours (corresponding to late E4 to early E8 stages) or 6.5 hours

318 (corresponding to E8-E16 stages) at 15 °C showed significantly increased lethality in
319 both *air-2(or207)* and *zen-4(or153)*, but not *spd-1(oj5)* (Table 1), which correlates
320 with the amount of cytokinesis failure observed. The few animals that were able to
321 hatch in *air-2(or207)* and *zen-4(or153)* mutants had severe morphogenesis defects
322 (data not shown). Mutant embryos shifted after the completion of all the
323 developmental divisions at the comma to 1.5-fold stage were largely rescued for
324 lethality and hatched at a rate similar to permissive temperature (Table 1). Therefore,
325 these results are consistent with the hypothesis that cytokinesis is essential for the
326 final stages of embryonic development during morphogenesis.

327 Next, we tested whether Aurora B kinase was required for the specialized E8-
328 E16 divisions and epithelial polarization. The *air-2(or207)* mutant has a high percent
329 cytokinesis failure within minutes after shifting to non-permissive temperature in one-
330 cell embryos (Severson et al., 2000), but does not show penetrant cytokinesis failures
331 unless shifted several hours in older embryos (Figure 4A). We first asked whether
332 microtubule organization at the midbody and apical surface required AIR-2 function.
333 Live cell imaging of *air-2(or207)* mutants expressing TBB-1::GFP shifted at the E4-
334 E8 stage demonstrated that spindle midzone microtubules were reduced relative to
335 wild-type E8 cells (Fig. 4 B-I, Video S6). Inactivation of *air-2(or207)* under these
336 conditions caused 27% of the observed E8 cells to fail cytokinesis, which causes these
337 cells to fail to polarize all nuclei at the midline (Fig. 4F-L). In cells that do not fail
338 cytokinesis, weak spindle midzone microtubules can be observed, which move to the
339 apical surface where microtubules quickly accumulate similar to WT (Fig. 4 B-I,
340 Video S6). In neighboring cells that fail cytokinesis, microtubule accumulation at the
341 apical midline is disrupted, which is most obvious when both left and right E8
342 divisions fail at the same time (Fig. 4 H, J, K, Video S6). Therefore, Aurora B kinase
343 is required for central spindle dynamics and completion of cytokinesis during the E8-
344 E16 divisions, which is required for normal nuclear polarization and accumulation of
345 microtubules at the apical midline.

346 To more clearly observe formation of the apical surface, we imaged the
347 dynamics of the adhesion complex during the E8-E16 divisions, which accumulates at
348 the apical surface during polarization to promote gut lumen formation (Achilleos et al.,
349 2010). We imaged the α-catenin homologue, HMP-1::GFP, a cytoplasmic component
350 of the cadherin-catenin adhesion complex that links cell-cell contacts with the actin

351 cytoskeleton. Previously, it was shown that polarity proteins recruit adhesion
352 complexes to cortical foci in the polar cortex (Achilleos et al., 2010), which associates
353 with centrosomes and moves with them to the apical midline (Feldman and Priess,
354 2012). We observed that HMP-1::GFP is also localized to the furrow from the onset
355 of furrow ingression, accumulates adjacent to spindle midzone microtubules and
356 moves together with the midbody to the apical surface (Fig. 5A-E, Movie S7).
357 Analysis of the first three E cell divisions also revealed localization of HMP-1::GFP
358 to the furrow and membrane adjacent to the midbody, suggesting a dynamic interplay
359 between adhesion and cytokinesis during the embryonic divisions (Fig. S4). In *air-*
360 *2(or207)* mutants, furrow HMP-1::GFP was reduced during cytokinesis (Fig. 5 F-J,
361 Video S7). In E8 *air-2(or207)* divisions that complete cytokinesis, HMP-1::GFP
362 signal normally accumulated at the apical midline (Fig. 5 F-J, Video S7). However, in
363 *air-2(or207)* E8 divisions that failed cytokinesis, accumulation of HMP-1::GFP was
364 significantly delayed especially when pairs of E8 daughters on opposite sides of the
365 midline both failed (Fig. 5 F-J, Video S7). Therefore, inactivation of Aurora B kinase
366 disrupts normal α-catenin dynamics during cytokinesis and delays accumulation of α-
367 catenin at the apical surface during polarization.
368 In order to understand the effect of cytokinesis failure on lumen formation, we
369 performed staining of the polarized gut using several apical markers. We shifted
370 mutant embryos around the transition between the E4-E8 stages to 26 °C and fixed at
371 the bean stage after intestinal polarization. We evaluated the formation of the apical
372 surface of the intestine by staining for the Ezrin-Radixin-Moesin homologue, ERM-1
373 (van Furden et al., 2004). We stained *air-2(or207)*, *zen-4(or153)* and *spd-1(oj5)* under
374 these conditions and observed penetrant cytokinesis defects in *air-2(or207*) and *zen-*
375 *4(or153)* but not *spd-1(oj5)* mutants (Fig. 6). In all cases, ERM-1 was localized to the
376 apical surface of the intestine and pharynx (Fig. 6 A-F). However, ERM-1 staining
377 was broadened, branched and/or discontinuous in *air-2(or207)* embryos (Fig. 6 B-D,
378 H). Disrupted ERM-1 staining was also observed in *air-2(or207)* embryos, which
379 were shifted at E4-E8 for 4.5-5 hours until the comma stage, indicating that these
380 defects are not resolved later in development (Fig. S5 B, D). Furthermore, the
381 intestine was highly mispositioned within the embryo as revealed by color-coded max
382 Z-projections (Figure 6 H) and the nuclei were often randomly positioned on the z-
383 axis compared with wild-type (Fig. 6 D-E inserts). The localization of other apical

384 markers, such as PAR-3, DLG-1 and IFB-2, were similarly disrupted, localizing to the
385 apical surface but in a disorganized way (Fig. S5 E-J). The *zen-4(or153)* embryos also
386 had highly penetrant branched and discontinuous apical ERM-1 staining that was
387 mispositioned within the embryo at a lower rate than the *air-2(or207)* mutants (Fig. 6
388 E, H and Fig. S5 C-D). The *spd-1(oj5)* embryos displayed a significant, but lower rate
389 and severity of lumen defects (Fig. 6 F-H) despite having no lethality (Table 1) and
390 minimal cytokinesis failures. Therefore, we conclude that proper execution of
391 cytokinesis is required for normal lumen formation in the gut.
392
393 **Apical midbody migration and AIR-2 apical localization in the pharynx**
394 We also noticed migration of the midbody and accumulation of midbody
395 proteins at the apical surface during the terminal divisions in the pharynx. Unlike the
396 intestine, which originates from a single blastomere that undergoes a very well
397 defined series of divisions, the pharynx has a more complicated structure, containing
398 more than 80 pharyngeal precursor cells (PPCs) that arise from both AB and MS
399 founder cells (Sulston et al., 1983). The PPCs organize into a double plate structure
400 prior to the final division, which occurs at around 310-325 minutes after the first
401 cleavage, and then polarize and undergo apical constriction to become wedge shaped
402 cells that form a lumen by 355 minutes (Rasmussen et al., 2013; Rasmussen et al.,
403 2012). To obtain optimal images of this large, complex structure, we filmed at least a
404 15-micron Z-depth section of the embryo from both dorsal and ventral aspects with
405 confocal microscopy (Figure 7, Video S8). We also filmed whole embryos with lattice
406 light sheet microscopy, which provides higher spatial resolution during the
407 pharyngeal cell division (Video S9). Similar to our observations in the intestine, PPCs
408 are in the final stages of cell division as they polarize, which has not been previously
409 described. PPCs undergo a symmetric furrowing event that yields a centrally placed
410 midbody between the two daughter cells (Fig. 7A and Video S8). Also similar to the
411 intestine, PPC midbodies migrate from their central position between daughter cells to
412 the apical midline of the forming pharyngeal bulb (Fig. 7 F, K, O and Video S9). In
413 PPC terminal divisions, AIR-2::GFP appears as a midbody flank structure that
414 migrates to the apical midline and persists at the apical surface after cyst formation
415 (Fig. 7 B-F and Video S9). ZEN-4::GFP appears on midbodies, migrates to the apical
416 surface, and is rapidly degraded, similar to the intestinal divisions (Fig. S6 A-E and
417 Video S8). NMY-2::GFP also labels midbodies and moves to the apical surface, but

418 remains localized to the apical surface during apical constriction (Fig. 7 G-K). Similar
419 to AIR-2, RAB-11 and tubulin accumulate and remain localized to the apical surface
420 after polarization (Fig. S6 F-K). We confirmed endogenous AIR-2 localization with
421 staining and show that it can be observed on the apical surface of the pharynx (Fig. S1
422 H-J). AIR-2 partially co-localized with PAR-6 at the apical membrane, which also
423 acquires γ-tubulin::GFP after polarization (Fig. S6 L-Q). Also similar to the intestinal
424 divisions, α-catenin (HMP-1::GFP) localizes to the furrow and adjacent to the
425 midbody as it migrates to the apical midline where it accumulates after polarization
426 (Fig. 7 L-O). Cytokinesis in the gut and pharynx show similar patterns where
427 midbodies migrate to the apical midline and specific midbody components, especially
428 AIR-2, remain localized at the apical cortex even after the midbody ring is removed.
429 Therefore, similar patterns of apical localization and midbody migration are observed
430 during epithelial polarization in the intestine and pharynx in *C. elegans*.
431
432 **Apical midbody clustering and Aurora B dendrite localization in sensilla**
433 **neurons**
434 Finally, we observed a unique form of cytokinesis during the final divisions of
435 the cells that make up the sensory neurons at the tip of the embryo. The *C. elegans*
436 amphid sensilla are a sensory organ that contains 12 neurons with dendrites that
437 extend processes through two sheath cells and the cuticle at the tip of the mouth.
438 During morphogenesis, amphid neurons bundle together, anchor at the tip of the
439 animal and migrate back to extend dendrites (Heiman and Shaham, 2009). From the
440 lineage of the 12 sensilla neurons, there are 10 precursor cell divisions that occur
441 between 280 and 400 minutes after the first cleavage (Sulston et al., 1983). These
442 terminal divisions include two daughter cell pairs (ADF/AWB and ASG/AWA) and
443 several where one daughter differentiates into a sensilla neuron while the other
444 daughter undergoes apoptosis (ADL, ASE, ASK, ASI), or differentiates into another
445 neuron (AWC, ASH, AFD, ASJ). Our observations show that these cells undergo a
446 unique form of cytokinesis just before they undergo dendrite morphogenesis (Fig. 8
447 A). These cells undergo a symmetrical furrowing event before midbodies form
448 centrally between the daughter cells (Fig. 8 B and Video S10-11). A group of at least
449 6 daughter cell pairs divide initially forming multiple midbodies as observed with
450 both confocal and lattice light sheet imaging (Fig. 8 C and Video S10-11). These

451 midbodies migrate together into a cluster over a 60-minute time window (Fig. 8 D).
452 AIR-2::GFP, RAB-11 and tubulin persist in these clusters (Fig. 8 D, Fig. S7 A-F),
453 while ZEN-4::GFP rapidly disappears during the midbody clustering process (Fig. 8 E
454 and Video S10). Endogenous AIR-2 can detected by staining in these lateral apical
455 clusters (Fig. S1 K-M). In contrast to ZEN-4::GFP, NMY-2::GFP migrates with the
456 midbody to the cluster and persists at the very tip of the dendrites (Fig. 8 F and Video
457 S10). We observe PAR-6 at the tip of the sensilla cluster, indicating that it is the
458 apical surface of these cells, which accumulates γ-tubulin::GFP similar to the pharynx
459 and gut (Fig. 8 G, Fig. S6 G-L). We also observe α-catenin (HMP-1::GFP) at the
460 furrow and midbody before it accumulates in the apical cluster of the sensilla neurons
461 and remains there during dendrite extension (Fig. 8 H-J). To our knowledge, this is
462 the first detailed examination of the division and initial steps of organization of these
463 neuronal cell precursors.
464 After formation of the cluster, we observe this apical region move and extend
465 anteriorly until it reaches the tip of the animal during the bean stage through the late
466 comma stage. AIR-2 remains localized along a substantial increasing length of the
467 dendritic extension during the entire elongation process, as does tubulin (Fig. 8 K-M,
468 Fig. S7 J-L, M-O and Video S12). As the amphid dendrites extend from the lateral
469 sides of the embryo, other foci of AIR-2 form within the anterior region of the embryo
470 and migrate toward the tip until six sensilla appear at the anterior tip (Fig. 8 M inset,
471 and Video S12). Although the individual cell divisions cannot be easily discerned in
472 this crowded anterior region, these data suggest that the sensilla in the tip of the
473 animal form through a similar process. These results demonstrate that directly after
474 cytokinesis a midbody migration event brings several midbody components to the
475 apical tip of the amphid dendrites, which remain localized there as dendrite extension
476 occurs. Neuronal cell polarization has been suggested to share mechanisms with
477 epithelial morphogenesis (McLachlan and Heiman, 2013), suggesting that these
478 modified cytokinesis events may play a role in cells that undergo epithelial
479 polarization. Therefore, the midbody migrates from its original position at the end of
480 furrowing to the apical surface in several developing tissues during morphogenesis.
481 Interestingly, Aurora B remains localized at the apical surface of these tissues well
482 after cytokinesis has occurred.
483

484 **Aurora B is required for proper dendrite formation**

485 Given our observation cytokinesis in the developing sensory neurons we tested
486 whether Aurora B kinase and other cytokinesis components were required for their
487 formation. *C. elegans* amphid neurons can take up lipophilic dyes such as DiI when
488 they form properly and generate cilia that are exposed to the environment (Hedgecock
489 and White, 1985; Perkins et al., 1986). We maintained embryos at the permissive
490 temperature (15 °C) and shifted them to the non-permissive temperature at different
491 embryo stages until they hatched, then we stained the surviving L1 larvae with DiI. In
492 wild-type, amphid neuron cell bodies, amphid dendrites, and phasmid neurons were
493 clearly labeled by DiI and appeared normal as expected (Fig. 9 A). In the *air-2(or207)*
494 mutant, we observed numerous defects in the subset of surviving embryos that did not
495 fail to hatch and became L1 larvae (Fig. 9 B-E). Animals with no observed DiI
496 staining were more common under longer inactivating conditions in the *air-2(or207)*
497 mutant (Table 2). All *zen-4(or153)* fail to hatch when shifted during E4-E8,
498 preventing analysis of DiI staining (Table 2). When shifted from the E8 stage, the few
499 surviving *zen-4(or153)* larvae show severe DiI staining defects, which was
500 dramatically reduced if embryos were shifted after the final divisions at the comma-
501 1.5 fold stage (Fig. 9 F, Table 2). The *spd-1(oj5)* animals still had weak defects
502 revealed by DiI staining despite having minimal cytokinesis failures, but never
503 showed a complete lack of staining (Fig. 9 I, Table 2). These data are consistent with
504 the hypothesis that proper execution of cytokinesis contributes to proper neurite
505 development. Therefore, cytokinesis and AIR-2 function especially are required late
506 in embryo development for epithelial polarization and morphogenesis of the lumen of
507 the gut and proper formation of the sensilla neurons.

508

509 **Discussion**

510 Our results have revealed complex and reproducible patterns of cytokinesis
511 during the invariant embryonic divisions in *C. elegans.* The entire invariant lineage
512 has been known for several decades and our results suggest that cytokinesis also
513 follows a specific pattern during the lineage. We observe reproducible alterations to
514 furrow symmetry, central spindle length, abscission timing, midbody movement and
515 inheritance. The traditional view of the embryo lineage is that cells are born and
516 subsequently undergo changes that produce the differentiated organization within a

517 tissue. However, our data demonstrate that cells in multiple tissues are completing
518 cytokinesis when they polarize during morphogenesis. We also demonstrate that
519 failures of cytokinesis disrupt proper epithelial polarization, disrupting nuclear
520 positioning and apical accumulation of microtubules and adhesion complexes. This
521 role for cytokinesis during polarization might explain why many cells in the lineage,
522 including several of the amphid neuronal precursors, divide and produce one daughter
523 cell that undergoes apoptosis instead of finishing the divisions earlier when the right
524 number of cells are generated. Such a role for a modified cytokinesis is observed later
525 in the Q neuroblast that generates a smaller a daughter cell that undergoes apoptosis,
526 which is prevented if the parameters of cytokinesis change (Ou et al., 2010). Given
527 that the entire cell is reconfigured during mitosis and that cytokinesis is the transition
528 period back into the interphase state, this is an ideal time window to reorganize
529 cellular architecture. Understanding how the developmental plasticity of cytokinesis is
530 regulated will be a fascinating question for future studies.

531 We observe consistent changes to the symmetry of furrow ingression where the
532 first mitosis is relatively symmetric and the second mitosis is highly asymmetric.
533 Previously, the furrow asymmetry in the first division was shown to be a consequence
534 of asymmetric accumulation of contractile ring components during ingression
535 (Maddox et al., 2007). The adhesion between cells may also reinforce this asymmetry
536 to drive the highly asymmetric furrow observed in the second round of divisions
537 (Padmanabhan and Zaidel-Bar, 2017). The dynamic localization of adhesion we
538 observe during cytokinesis at several stages of development suggest that adhesion
539 may control cellular interactions during the disruptive process of anaphase spindle
540 elongation and cytokinesis to maintain cellular positioning in the embryo. Whether
541 due to cell intrinsic or extrinsic factors, the asymmetric furrows have previously been
542 postulated to drive efficient furrowing or help maintain proper cell-cell contacts
543 during cytokinesis (Maddox et al., 2007; Morais-de-Sa and Sunkel, 2013). Our data
544 suggest another hypothesis: the asymmetric furrow may be required for the AB
545 midbody to be engulfed by EMS instead of either daughter cell. Given that the
546 midbody has been proposed to deliver signals to cells that inherit it, it is worth noting
547 that the MS cell collects up to four midbodies over time (Singh and Pohl, 2014). We
548 see relatively symmetric furrowing in several tissues later in morphogenesis. This is
549 unexpected because an asymmetric furrow would be sufficient to position the

550 midbody at the nascent apical surface. Given that the polarization mechanisms are not
551 completely understood, for example the extracellular matrix component laminin is
552 required in the pharynx but not the intestine (Rasmussen et al., 2012), the symmetrical
553 furrow followed by midbody migration may be important for defining and positioning
554 the apical surface. Perhaps there is no good reference for an asymmetric furrow to
555 position the midbody at the apical surface prior to epithelial polarization in cells in
556 different locations. We hypothesize that lumen formation in the gut and pharynx is
557 analogous to that described in MDCK cells with the formation of a midbody-derived
558 apical-membrane initiation site with the addition of midbody migration for correct
559 positioning of this domain (Li et al., 2014).

560 The coordinated, directed movement of the midbody we observe in several
561 tissues represents a new phenomenon during cytokinesis. Our data also suggest that
562 abscission has not taken place before the midbody migrates in the intestine. This
563 would mean that the two daughter cells polarize while connected at the midbody,
564 which might facilitate their reorganization. These data are somewhat different from
565 what is observed in already polarized epithelia where the furrow constricts from the
566 basal to the apical surface to position the midbody. We demonstrate that Aurora B is
567 required for successful completion of cytokinesis and polarization of microtubules
568 and adhesion. In the future it will be important to specifically prevent the movement
569 of the midbody and determine the affect it has on the polarization process. We
570 hypothesize that midbody migration to the apical surface is involved in cells that
571 polarize during a mesenchyme to epithelial transition. Previously, midbodies have
572 been shown to reposition after forming under normal or mutant conditions (Bernabe-
573 Rubio et al., 2016; Herszterg et al., 2013; Morais-de-Sa and Sunkel, 2013; Singh and
574 Pohl, 2014), but this phenomena is only appreciated in isolated cases and poorly
575 understood. The entire cortex is controlled by several actin cytoskeletal regulators in
576 order to perform cytokinesis (Jordan and Canman, 2012), perhaps this is also
577 employed to control the movement of the midbody. In the future, it will be important
578 to investigate how the midbody moves to the apical surface and how various delivered
579 proteins contribute to polarization.

580 In the tissues we investigated, the cells are undergoing their terminal cell
581 division before morphogenesis, although some cells like those in the gut undergo
582 post-embryonic divisions. These cells are also undergoing epithelial polarization and

583 a mesenchymal to epithelial transition. After midbody movement, RAB-11, AIR-2,
584 microtubules and possibly other molecules are recruited to the apical surface.
585 Certainly, these different tissues have unique gene expression programs, part of which
586 might involve proteins delivered to the midbody and the apical surface. For example,
587 a transmembrane protein that binds to an extracellular partner is expressed in the tip
588 of the dendrites in amphid sensilla, which is required to maintain dendrite attachment
589 at the tip of the embryo (Heiman and Shaham, 2009). It is unknown how this protein
590 localizes to the tip of the dendrite, but one speculative possibility given our
591 observations that midbody components localize to the same site is that it could be
592 delivered through cytokinesis-directed membrane trafficking. Delivering proteins
593 through the midbody was observed in neuroepithelial cells where a stem cell marker
594 protein is released into the extracellular environment in released midbody remnants
595 (Dubreuil et al., 2007). Later in life, the worm releases exosomes from the sensory
596 cilia that form at the tip of the dendrites of the sensilla for communication between
597 animals (Wang et al., 2014a). Perhaps the initial secretory apparatus built during
598 cytokinesis to promote cell division is recruited to the apical surface of these neurons
599 to enable exosome release. Further investigation is required to define the molecular
600 contributions provided by the midbody to the apical surface of these tissues.
601 Once the midbody moves to the apical surface, we observe that different
602 components of the midbody have different fates, which is an unexpected and novel
603 observation. Typically, once the midbody is abscised from the cell, it is thought that
604 most midbody proteins are discarded with the remnant, as observed in the early
605 embryo divisions. Aurora B kinase remains at the apical surface well after other
606 midbody components like ZEN-4 are removed. The limit of the resolution of light
607 microscopy does not allow us to characterize in detail how this occurs. The most
608 likely model is that the central midbody bulge is cut from the plasma membrane and
609 flank proteins like Aurora B, RAB-11, and microtubules are left behind. Among the
610 many mitotic functions of Aurora B, it is a critical regulator of the timing of
611 abscission (Mathieu et al., 2013; Steigemann et al., 2009). Based on our observations
612 of midbody flank microtubules and the timing of midbody ring internalization,
613 abscission likely occurs after the midbody migration event, and the delay in
614 abscission might require Aurora B activity. Delayed abscission by Aurora B kinase in
615 mouse embryos was shown to maintain interphase bridges that mediate RAB-11
616 dependent delivery of cell adhesion molecules to apical membranes (Zenker et al.,

617 2017). We find that inhibition of Aurora B diminishes spindle midzone microtubules
618 and leads to reduced adhesion at the furrow and midbody during cytokinesis, which is
619 consistent with such a mechanism operating during epithelial polarization. Aurora B
620 was recently shown to be regulated by an atypical cadherin in early zebrafish embryos
621 to regulate the spindle midzone microtubule organization (Chen et al., 2018), further
622 suggesting reciprocal regulation between adhesion and cytokinesis. Aurora B also
623 regulates a number of cytoskeletal regulators during cytokinesis that control cell
624 shape (Ferreira et al., 2013; Floyd et al., 2013; Goto et al., 2003; Kettenbach et al.,
625 2011), and it will be important to determine whether any are involved with the events
626 we observed. In the intestine, the central spindle elongates dramatically as the
627 midbody migrates, which might also be regulated by Aurora B (Bastos et al., 2013).
628 Spindle midzone regulation is controlled by altered expression of the central spindle
629 protein PRC-1 (the homologue of *spd-1*) in the *Xenopus* embryo, which correlates
630 with changes to furrow ingression and midbody behavior (Kieserman et al., 2008).
631 While we observe the centralspindlin component ZEN-4 becoming rapidly
632 internalized with the midbody in the three tissues, it was previously implicated in
633 morphogenesis of the epidermis and pharynx (Hardin et al., 2008; Portereiko et al.,
634 2004; Von Stetina et al., 2017). It remains to be determined whether this role is
635 related to the dynamics of cytokinesis or a cytokinesis-independent function of ZEN-4
636 as previously suggested. Therefore, further study will be required to understand the
637 role of the spindle midzone components during the specialized cytokinesis events that
638 occur during morphogenesis.
639 In the sensilla, the centriole moves to the tip of the dendrite to form the base of
640 the sensory cilia of these neurons (Dammermann et al., 2009; Nechipurenko et al.,
641 2017; Perkins et al., 1986). Multiple central spindle proteins localize to the base of
642 cilia in *Xenopus* epithelial cells and are required for cilia morphology after the
643 divisions are completed in *C. elegans* (Kieserman et al., 2008; Smith et al., 2011).
644 Additionally, loss of Aurora B kinase causes aberrant neuronal axon morphology, and
645 overexpression of Aurora B causes extended axonal outgrowth in zebrafish (Gwee et
646 al., 2018). At the apical surface of the gut, γ-tubulin and other pericentriolar material
647 is delivered from the centrosome while the centrioles are discarded (Feldman and
648 Priess, 2012). The gut apical membrane ultimately becomes elaborated with microvilli
649 (Feldman and Priess, 2012; Leung et al., 1999). We also observed γ-tubulin at the
650 apical surface of the pharynx and sensilla dendrites. Therefore, different material

provided by the midbody and centrosome may contribute to the cytoskeletal architecture of the apical surface depending on the needs of each tissue. Delineating the precise relationship between these two organelles and deciphering how cytokinesis contributes to proper cellular reorganization during morphogenesis will be a major focus of future studies.

Acknowledgements

Lattice light sheet microscopy was performed in collaboration with the Advanced Imaging Center at HHMI Janelia Research Campus, a facility jointly supported by the Gordon and Betty Moore Foundation and the Howard Hughes Medical Institute. We appreciate the CGC and Wormbase funded by the NIH Office of Research Infrastructure Programs (P40 OD010440) and National Human Genome Research Institute (U41 HG002223), which provided some *C. elegans* strains and genome information. We are grateful to members of the Bembenek laboratory for productive discussion, reagent preparation and handling strains. We also thank Dr. Max Heiman, Dr. Zhirong Bao for discussions and Dr. Don Fox, Dr. John White, Dr. John Heddleston, Dr. Heidi Hehnley-Chang, Lindsay Rathbun, and Erica Colicino for critical feedback on the manuscript. Funding was provided by the Ministry of Science Technology of Taiwan (105-2119-M-001-026-MY2) to C.B.C., the Howard Hughes Medical Institute to E.B., and NIH R01 GM114471 to J.N.B.

672 **Figure Legends**

673 **Figure 1. Cytokinesis in the first two mitotic divisions**

674 (A) Illustration of cytokinesis in the first two mitotic divisions indicating the invariant fate of
675 the midbody after division. Orange shapes indicate the first midbody, while blue shapes
676 indicate the AB midbody. (B-F) Cytokinesis labeled with AIR-2::GFP (green, PH::mCherry
677 and H2B::mCherry in magenta). During late anaphase, Aurora B localizes on the central
678 spindle (B) which condenses into the midbody flank (C, orange arrowhead) and remains on
679 the midbody until it is internalized by the AB daughter cell (D, orange arrowhead). During the
680 second mitosis, the furrow is highly asymmetric and sweeps the central spindle against the
681 EMS boundary, where the midbody forms (E, blue arrowhead). EMS engulfs the midbody
682 instead of either of the AB daughter cells (F, blue arrowhead). (G-K) NMY-2::GFP (green,
683 PH::mCherry in magenta) show localization to the furrow (G) and midbody ring (H-K). (L-P)
684 ZEN-4::GFP (green, PH::mCherry in magenta) appears on the central spindle (L) and the
685 midbody (M-P). (Q-U) RAB-11::mCherry (green) co-localized with AIR-2::GFP (magenta)
686 briefly at the midbody, but does not remain on the midbody once it is internalized into cytosol
687 (R-U). (V-X) Quantification of furrow asymmetry, measurement illustrated in V, W. (X)
688 Furrow asymmetry parameter is significantly greater in second cell division. Scale bar, 10 μm.

689

690 **Figure 2. Midbody migration and Aurora B apical localization in the E8-E16 intestinal**
691 **divisions**

692 (A) Diagram of cytokinesis in the intestinal E8-E16 mitotic divisions indicating localization
693 of Aurora B (green, midbody ring in magenta). (B-D) Lattice light sheet imaging of E8-E16
694 intestinal cell divisions in embryos expressing AIR-2::GFP (green) with PH::mCherry
695 (magenta). AIR-2::GFP labels midbodies (labeled 1-8 in B) that form in the middle of E8
696 daughter cell pairs and then migrate (arrowheads, C) to the nascent apical membrane where it
697 persists well after polarization is complete (D). (E-G) Spinning disc confocal microscopy of
698 AIR-2::GFP (green) with H2B::mCherry and PH::mCherry (magenta) showing midbody
699 migration (F) and apical localization (G). (H) Image series of Epla division with AIR-2::GFP
700 (green, PH::mCherry in magenta) starting in prometaphase, clearly indicating midbody
701 formation (t=0) and migration to apical midline. (I-K) NMY-2 (green, microtubules in
702 magenta) localizes to furrows, then midbody rings (labeled 1-8 in F) that move to the midline
703 (arrowheads, J) but do not persist (rectangle box in K). (L) Montage showing a single NMY-
704 2::GFP labeled midbody migrating to midline. (M-N) Single plane imaging of midbody
705 dynamics in individual intestine cell shows extension of the central spindle and apical
706 membrane localization of AIR-2::GFP (M) and rapid internalization of ZEN-4::GFP (N) to

707 the cytosol. (O) Quantification of midline perdurance of different midbody components
708 (measured from the end of furrowing to internalization or loss of signal). (P) Illustration of E8
709 division and (Q) quantification of the ratio of maximal midbody flank length to cell length in
710 different divisions. Scale bar, 10 µm. Time shown in minutes:seconds. Error bars indicate
711 standard deviation of the mean.

712

713 **Figure 3. Abscission is delayed during gut epithelial polarization**

714 Spindle midzone microtubule dynamics were imaged during different cell divisions to assess
715 abscission timing. (A-B) AIR-2::GFP (magenta) and β-tubulin TBB-1::mCherry (green)
716 colocalize at the central spindle during anaphase and furrowing in the first cell division. AIR-
717 2::GFP persists at the midbody after microtubules are lost, which indicates rapid abscission
718 timing (B). (C-D) AIR-2::GFP (magenta) and β-tubulin TBB-1::mCherry (green) colocalize
719 on the central spindle of the AB cell that is swept adjacent to EMS after highly asymmetric
720 furrowing. Microtubules are lost quickly like the first division (D). (E-G) Tubulin TBB-
721 1::mCherry (green) and AIR-2::GFP (magenta) localize to an extended flank region during
722 intestinal midbody migration (F, arrowhead). (G) Tubulin and AIR-2 persist at the apical
723 membrane after polarization (rectangle box). (H) Single z-plane imaging of midbody flank
724 microtubules (arrowheads) during Epra cell division and midbody migration. The extended
725 flanking microtubules persist at least 3 times longer than earlier divisions throughout the
726 migration process until they can no longer be distinguished from other microtubules at the
727 apical surface. (I) Quantification of tubulin persistence time at the central spindle during
728 different cell divisions. Scale bar, 10 µm. Error bars indicated standard deviation of the mean.

729

730 **Figure 4**. **Aurora B is required for E8-E16 cytokinesis and epithelial polarization**

731 Timeline of cell division events in the intestine (upper timeline) and the temperature shift
732 strategy inactivating mutants from the end of the E4-E8 division through E8-E16 cytokinesis
733 (A). (B-E) Imaging of microtubules (TBB-1::GFP, green) together with H2B::mCherry and
734 PH::mCherry (magenta) shows spindle midzone microtubules (arrows, C) that migrate to the
735 apical midline (D) where microtubules accumulate after polarization (E). In Aurora B mutant
736 embryos (F-I), spindle midzone microtubules are diminished (G, solid arrowhead). Frequent
737 cytokinesis failures occur (G, H, open arrowheads) and nuclei fail to migrate to the apical
738 midline (G-I, red asterisks). (J) Quantification of defects in Aurora B mutant E8-E16
739 divisions showing significant cytokinesis failures where most cells that failed also have
740 nuclear polarization defects. Of the 11 embryos observed, five have apical microtubule

741 accumulation defects. The low incidence of chromosome segregation defects indicate weak
742 Aurora B inactivation compared with early embryo divisions in this mutant. (K) Diagram of
743 failure patterns of pairs of E8-E16 divisions on opposite sides of midline and observed
744 consequence on microtubule accumulation (green) at apical midline. (L) Quantification of
745 individual cell division failures and incidence of discontinuous microtubule accumulation at
746 the apical midline after polarization. Scale bar, 10 μm.

747

748 **Figure 5**. **Aurora B is required for adhesion dynamics and timely apical adhesion**
749 **accumulation during E8-E16 gut cytokinesis**

750 Adhesion dynamics during E8-E16 intestinal division and polarization. (A-D) HMP-1::GFP
751 (α-catenin, green, microtubules in magenta) localizes to the furrow and membrane adjacent to
752 the midzone microtubules in the midbody (B, arrowhead) during cytokinesis. HMP-1::GFP
753 localizes with the midbody as it migrates to the apical surface where it accumulates (C, D). (E)
754 High temporal resolution imaging of HMP-1::GFP shows furrow and midbody accumulation
755 (arrowheads) during cytokinesis and localization adjacent to midzone microtubules as they
756 migrate to the apical midline. (F-I) Aurora B mutants disrupt adhesion dynamics. HMP-
757 1::GFP is reduced on the furrow and midbody (F,G, open arrowhead). When both cells fail
758 cytokinesis (G, H, open arrowheads indicate failures) on opposite sides of the midline, HMP-
759 1 accumulation is delayed (dashed bracket indicates midline between two failed E8 gut cells,
760 solid bracket indicates successful E8 division with apical accumulation). (I) HMP-1 signal
761 eventually accumulates along the midline. (J) Kymograph of HMP-1::GFP in Aurora B
762 mutant E8 cells that fail cytokinesis (open arrowheads indicate furrow regression) shows
763 reduced localization to the furrow, midbody and delayed apical accumulation. (K)
764 Quantification of defects in Aurora B mutant E8-E16 divisions showing significant defects in
765 HMP-1::GFP accumulation with cytokinesis failures. (L) Diagram of cytokinesis failures in
766 pairs of E8-E16 divisions on opposite sides of midline and observed consequence on adhesion
767 accumulation (green) at apical midline. (M) Quantification of individual cell division failures
768 and incidence of discontinuous adhesion accumulation at the apical midline after polarization.
769 Scale bar, 10 μm.

770

771 **Figure 6. Gut morphogenesis is disrupted in cytokinesis mutants**

772 Staining of apical markers reveals gut morphology after E8-E16 division and polarization. (A)
773 ERM-1 staining in wild-type bean stage embryos is enriched at the apical midline of the
774 intestine (dotted rectangle). Maximum z-projected images color-coded according to Z-depth

775 (using FIJI temporal-color code plugin, scale shown in F) to visualize the three-dimensional
776 position of ERM-1 and nuclei, which are mostly in a narrow range of Z-depth (A-F, H). In
777 *air-2(or207)*, multiple defects are observed, including mispositioning of the entire intestine
778 (B-D), branches in the apical surface (B), gaps in the apical surface creating a discontinuous
779 lumen (C), or broader staining of ERM-1 (D). (E) The *zen-4(or153)* mutant causes many of
780 these phenotypes, including branching of the apical surface and randomly positioned nuclei.
781 (F) Subtle lumen and nuclei position defects are observed in *spd-1(oj5)* embryos. (G)
782 Quantification of apical defects observed by ERM-1 staining in the different mutants. (H)
783 Quantification of the defective z-plane distribution of the apical surface in the different
784 mutants. The more colors a lumen has in the projection, the more skewed in the Z-axis it is
785 within the embryo. Scale bar, 10 μm.

786

787 **Figure 7. Cytokinesis During Pharyngeal Precursor Cell Polarization**

788 (A) Illustration of the mesenchymal to epithelial transition of pharyngeal precursor cells
789 (PPCs) showing cell division and dynamics of Aurora B (green, midbody ring in magenta).
790 (B-E) PPC division labeled with AIR-2::GFP (green, H2B::mCherry in magenta) from both
791 ventral (B-D) and dorsal (E) views. AIR-2::GFP localizes to chromatin in metaphase (B) and
792 moves to the central spindle in anaphase (C) and appears on the midbody which moves
793 toward the midline (D). AIR-2 persists at the apical surface for an extended time (E). (F)
794 Image series showing an AIR-2::GFP labeled midbody migrating toward the midline. (G-J)
795 Imaging NMY-2 (green, TBB-1::mCherry in magenta), shows the movement of the midbody
796 to the midline (I, K). NMY-2 accumulates at the apical midline during apical constriction (J).
797 (L-N) During cytokinesis, α-catenin (HMP-1::GFP, green, tubulin in magenta) accumulates
798 on the furrow (arrowhead in L) and adjacent to the midbody (arrowhead, M) before
799 accumulating at the midline (N). (O) Shows kymograph of HMP-1::GFP at the furrow and
800 midbody, which migrates to the apical midline where HMP-1 ::GFP accumulates. Time
801 shown in minutes: seconds. Scale bar, 10 μm.

802

803 **Figure 8**. **Midbody components label dendrites of sensilla neurons**

804 (A) Diagram of sensilla precursor cell (SPC) divisions and the localization of the AIR-2::GFP
805 at the midbody during cytokinesis until the apical clustering during polarization. (B-D)
806 Cytokinesis in SPCs in the anterior lateral region of the embryo expressing AIR-2::GFP
807 (green, H2B::Cherry in magenta) gives rise to multiple midbodies (arrowheads B,C) that
808 cluster together at the lateral sides of the embryos (D). (E) The midbody ring marker ZEN-

809 4::GFP (green, microtubules in magenta) is internalized and degraded before the cluster forms,
810 which is also concentrated with microtubules (arrowheads). (F) NMY-2::GFP (green,
811 microtubules in magenta) localizes to midbodies that cluster and remains at the tip of the
812 dendrite as it extends. (G) PAR-6::mCherry (green, AIR-2::GFP in magenta) localizes to tip
813 of the cluster (arrowheads) and persists at the tip of the dendrites as they extend, indicating
814 that this is the apical surface of these cells. (H-J) HMP-1::GFP accumulates at the furrow and
815 midbody (arrowhead, H, I) during sensilla precursor divisions and accumulates at the cluster
816 and remains at the tip during dendrite extension (J). (K-M) After the apical cluster forms,
817 AIR-2::GFP remains at the tip (red arrowheads) as the cells migrate to the nose of the animal.
818 AIR-2::GFP also labels a substantial portion of the length of the dendrite as they extend (M).
819 Insert in (M) is a rotated max z-projection showing the anterior end of the animal after
820 multiple sensilla form. Time shown in minutes:seconds. Scale bar, 10 µm.

821

822 **Figure 9**. **Cytokinesis mutants have disrupted sensilla neuron morphology**

823 Visualizing dendrite and neuron morphology by DiI staining in surviving larvae after shifting
824 mutants to 25 °C at the E4 or E8 stage until hatching. (A) In wild-type animals, two dendrite
825 bundles can be clearly observed as well as amphid and phasmid neurons. (B-E) Hatched
826 mutant larvae displayed a variety of neurite defects, including No-DiI signal (B, F), Weak
827 signal (C, G), dendrite shape and positioning defects (D) and additional diffuse staining
828 throughout the head of the animal (E, H, I).
829

830 **Materials and Methods**

831 ***C. elegans* Strains**

832 *C. elegans* strains were maintained with standard protocols. *C. elegans* strains
833 expressing midbody proteins driven by the *pie-1* promoter are listed in Table 2. All
834 temperature-sensitive mutants were obtained from the Caenorhabditis Genetics Center.
835

836 **Embryo Preparation and Imaging**

837 For live imaging, young gravid hermaphrodites were dissected in M9 buffer
838 containing polystyrene microspheres and sealed between two coverslips with vaseline
839 (Pohl and Bao, 2010). Live cell imaging was performed on a spinning disk confocal
840 system that uses a Nikon Eclipse inverted microscope with a 60 X 1.40NA objective,
841 a CSU-22 spinning disc system, and a Photometrics EM-CCD camera from Visitech
842 International. Images were acquired by Metamorph (Molecular Devices) and analyzed
843 by ImageJ/FIJI Bio-Formats plugins (National Institutes of Health) (Linkert et al.,
844 2010; Schindelin et al., 2012). Whole embryo live imaging was performed on a lattice
845 light sheet microscopes housed in the Eric Betzig lab, Bi-Chang Chen lab, or the
846 Advanced Imaging Center at HHMI Janelia. The system is configured and operated as
847 previously described (Chen et al., 2014). Briefly, embryos were dissected out and
848 adhered to 5 mm round glass coverslips (Warner Instruments, Catalog # CS-5R).
849 Samples were illuminated by lattice light-sheet using 488 nm or 560 nm diode lasers
850 (MPB Communications) through an excitation objective (Special Optics, 0.65 NA,
851 3.74-mm WD). Fluorescent emission was collected by detection objective (Nikon,
852 CFI Apo LWD 25XW, 1.1 NA), and detected by a sCMOS camera (Hamamatsu Orca
853 Flash 4.0 v2). Acquired data were deskewed as previously described (Chen et al.,
854 2014) and deconvolved using an iterative Richardson-Lucy algorithm. Point-spread
855 functions for deconvolution were experimentally measured using 200nm tetraspeck
856 beads adhered to 5 mm glass coverslips (Invitrogen, Catalog # T7280) for each
857 excitation wavelength.
858

859 **Immunostaining Assay in *C. elegans* Embryos**

860 Apical marker staining was performed with the freeze-crack methanol protocol
861 (Leung et al., 1999). Immunostaining with anti-AIR-2 antibodies was performed as
862 described (Schumacher et al., 1998). Primary antibodies and (dilutions) used were
863 anti-ERM-1 (1:200); P4A1/PAR-3 (1:200); DLG-1 (1:200); MH33 (1:150); AIR-2

(1:50). 1:200-400 dilutions of Alexa 588 and 468 secondary antibodies were used in the study. To stain temperature-sensitive mutants, two-cell stage embryos were dissected from gravid worms, mounted in 10 μL of M9 buffer, and kept cold on ice. The two-cell stage embryos were incubated at 15 °C for 4-7 hours until specific stages, then shifted to the restrictive temperature (25 °C) for 2-4 hours and stained as described above.

DiI staining in *C. elegans*

DiI staining of wild-type and temperature sensitive mutants was done as previously described (Tong and Burglin, 2010). Two-cell stage embryos were incubated at 15 °C for 6.5~7 hours until they reached the polarized E16 stage, then shifted to the restrictive temperature (25 °C) with 1:200 dilution of stock DiI dye solution containing 2 mg/mL DiI in dimethyl formamide for 18-24 hours. Hatched larvae were transferred to M9 and washed twice in M9 before mounting in 25 mM levamisole on 2% agar pads for imaging.

Temperature-Shift Experiments

Temperature-sensitive mutants were maintained at 15 °C. To perform temperature shifts on staged embryos, gravid adults were transferred to a dissection chamber (< 4 °C), which was precooled in ice bucket, with 20 μL of ice-cold M9 Buffer. Two-Cell stage embryos were quickly transferred (within a 5-10 minute time window) via mouth pipette (Aspirator tube assemblies, Sigma) to Fisherbrand Hanging Drop Slides (Catalogue #12-560B) on ice. The slide was placed into a humidified chamber and incubated at 15 °C until the appropriate stages were reached and then shifted to 26 °C. Incubation times were determined based on *C. elegans* embryonic lineage timing and adjusted according to DAPI staining to ensure each mutant was shifted at a similar stage of embryo development. To inactivate *air-2(or207)*, mutant embryos were incubated for 5 hours at 15 °C and shifted to 26 °C for 3 hours to reach the bean stage or 5 hours at 26 °C to reach the comma stage. This was the minimum amount of time to shift embryos to non-permissive temperature and observe significant cytokinesis defects by the E8-E16 division, indicating significant reduction of AIR-2 function. Most embryos reached the E4-E8 division at the time of the shift. By live imaging we found that there was little disruption of the E4-E8 division under these conditions

897 since (n=4/5) *air-2(or207)* embryos have 8 normal E8 cells. N2*, spd-1(oj5)*, and *zen-*
898 *4(or153)* embryos were incubated for 4.5 hours at 15 °C to reach E4-E8 stage,
899 followed by 3 hours at 26 °C to reach the bean stage and 5 hours at 26 °C to reach the
900 comma stage. To shift embryos at the comma stage*, air-2(or207)* embryos were
901 incubated for 12 hours at 15 °C and N2*, spd-1 (oj5) and zen-4(or153)* embryos were
902 incubated 11-11.5 hours at 15 °C.

903

904

905

906 **Table 1. Hatch rate of temperature sensitive mutants dissected at the two cell**
907 **stage.**

908

Stage Before Shifting	Genotype	Hatch Rate % (Hatch Embryos/Total)
15 °C Forever	N2	100% (32/32)
	air-2(or207)	53.6% (37/69)
	zen-4(or153)	100% (28/28)
	spd-1(oj5)	100% (35/35)
E4-E8	N2	100% (26/26)
	air-2(or207)	6.3% (2/32)
	zen-4(or153)	0% (0/57)
	spd-1(oj5)	100% (48/48)
E8-E16	N2	100% (45/45)
	air-2(or207)	14.4% (13/90)
	zen-4(or153)	10.1% (10/99)
	spd-1(oj5)	100% (83/83)
Comma-1.5 Fold	N2	100% (36/36)
	air-2(or207)	33.7% (31/92)
	zen-4(or153)	85.7% (54/63)
	spd-1(oj5)	100% (27/27)

909

910 **Table 2. Quantification of DiI Staining of Temperature-Sensitive Mutants**

911

Stage Before Shifting	Genotype	No DiI Signal	Weak DiI signal	Shape & Position Defect	Extended DiI Staining
15 °C Forever	N2	0% (0/32)	0% (0/32)	0% (0/32)	0% (0/32)
	air-2(or207)	2.7% (1/37)	8.1% (3/37)	2.7% (1/37)	0% (0/37)
	zen-4(or153)	0% (0/18)	0% (0/18)	0% (0/18)	0% (0/18)
	spd-1(oj5)	0% (0/34)	0% (0/34)	0% (0/34)	0% (0/34)
E4-E8	N2	0% (0/10)	0% (0/10)	0% (0/10)	0% (0/10)
	air-2(or207)	50% (1/2)	0% (0/2)	50% (1/2)	0% (0/2)
	zen-4(or153)	0% (0/0)	0% (0/0)	0% (0/0)	0% (0/0)
	spd-1(oj5)	0% (0/44)	4.5% (2/44)	9.1% (4/44)	6.8% (3/44)
E8-E16	N2	0% (0/29)	0% (0/29)	0% (0/29)	0% (0/29)
	air-2(or207)	16.7% (2/12)	58.3% (7/12)	58.3% (7/12)	0% (0/12)
	zen-4(or153)	77.8% (7/9)	11.1% (1/9)	22.2% (2/9)	0% (0/9)
	spd-1(oj5)	0% (0/59)	0% (0/59)	8.5% (5/59)	5.1% (3/59)
Comma-1.5 Fold	N2	0% (0/21)	0% (0/21)	0% (0/21)	0% (0/21)
	air-2(or207)	6.9% (2/29)	10.3% (3/29)	0% (0/29)	13.8% (4/29)
	zen-4(or153)	0% (0/53)	0% (0/53)	0% (0/53)	22.6% (12/53)
	spd-1(oj5)	0% (0/18)	0% (0/18)	0% (0/18)	33.3% (6/18)

912 **Table 3. Strains used in this study.**

Strain	**Genotype**
N2	Bristol (wild-type)
EKM48	*unc-119(ed3) iii; ojIs51 [Ppie-1::GFP::air-2; unc-119(+)]*
EKM50	*unc-119(ed3) iii; ojIs51 [Ppie-1::GFP::air-2; unc-119(+)]; ItIs37 [Ppie-1::mCherry::his-58 (pAA64); unc-119(+)] iv; ItIs44 [Ppie-1::mCherry::PH (PLC1delta1); unc-119(+)]v*
EKM51	*unc-119(ed3) iii; ojIs51 [Ppie-1::GFP::air-2; unc-119(+)]; ItIs37 [Ppie-1::mCherry::his-58 (pAA64); unc-119(+)] iv*
EKM52	*unc-119(ed3) iii; ojIs51 [Ppie-1::GFP::air-2; unc-119(+)]; ItIs44 [Ppie-1::mCherry::PH (PLC1delta1); unc-119(+)] v*
JAB23	*unc-119(ed3) iii; ojIs51 [Ppie-1::GFP::air-2; unc-119(+)]; weIs21 [pJA138 (pie-1::mCherry::tub)]*
JAB60	*unc-119(ed3) iii; ojIs51 [Ppie-1::GFP::air-2; unc-119(+)]; pwIs476 [Ppie-1::mCherry::rab-11]*
JAB116	*unc-119(ed3) iii; weIs21 [pJA138 (Ppie-1::mCherry::tub)]; unc-119(+)]; zuIs45 [nmy-2::NMY-2::GFP; unc-119(+)] v*
NWG002	*unc-119(ed3) iii; ItIs44 [Ppie-1::mCherry::PH (PLC1delta1); unc-119(+)]v; zuIs45 [nmy-2::NMY-2::GFP; unc-119(+)] v*
JAB24	*zen-4(or153ts) iv; xsEx6 [zen-4::GFP; rol-6 (su1006)]; unc-119(ed3) iii; weIs21 [pJA138 (pie-1::mCherry::tub)]*
JAB34	*zen-4(or153) iv; xsEx6 [zen-4::GFP; rol-6 (su1006)]; unc-119(ed3) iii; ItIs44 [Ppie-1::mCherry::PH (PLC1delta1); unc-119(+)] v*
JAB32	*unc-119(ed3) iii; ddIs26 [Ppie-1::mCherry::T26E3.3; unc-119(+)]v; ojIs51 [Ppie-1::GFP::air-2; unc-119(+)]*
EU630	*air-2(or207) i.*
EU716	*zen-4(or153) iv.*

WH12	*spd-1(oj5) i.*
WH421	*unc-119(ed3) iii; ojIs51 [Ppie-1::GFP::air-2; unc-119(+)];spd-1 (oj5) i.*
JAB39	*unc-119(ed3) iii; ruls32III;dd156[tbg-1::GFP;unc-119(+)];; ojIs51 [Ppie-1::GFP::air-2; unc-119(+)];spd-1 (oj5) i.*
JAB52	*unc-119(ed3) iii; ruls32III;dd156[tbg-1::GFP;unc-119(+)]; ruls32[Ppi-1::GFP::His-58; unc-119(ed3); weIs21 [pJA138 (pie-1::mCherry::tub)]*

913

914 Bibliography

915 Achilleos, A., Wehman, A.M., and Nance, J. (2010). PAR-3 mediates the initial clustering
916 and apical localization of junction and polarity proteins during C. elegans intestinal epithelial
917 cell polarization. Development *137*, 1833-1842.
918 Ai, E., Poole, D.S., and Skop, A.R. (2009). Rack-1 Directs Dynactin-dependent RAB-11
919 Endosomal Recycling during Mitosis in Caenorhabditis elegans (vol 20, 1629, 2009). Mol
920 Biol Cell *20*, 5036-5036.
921 Albertson, R., Riggs, B., and Sullivan, W. (2005). Membrane traffic: a driving force in
922 cytokinesis. Trends Cell Biol *15*, 92-101.
923 Amini, R., Goupil, E., Labella, S., Zetka, M., Maddox, A.S., Labbe, J.C., and Chartier, N.T.
924 (2015). C. elegans Anillin proteins regulate intercellular bridge stability and germline
925 syncytial organization (vol 206, pg 129, 2014). J Cell Biol *209*, 467-467.
926 Bai, X.F., and Bembenek, J.N. (2017). Protease dead separase inhibits chromosome
927 segregation and RAB-11 vesicle trafficking. Cell Cycle *16*, 1902-1917.
928 Bastos, R.N., Gandhi, S.R., Baron, R.D., Gruneberg, U., Nigg, E.A., and Barr, F.A. (2013).
929 Aurora B suppresses microtubule dynamics and limits central spindle size by locally
930 activating KIF4A. J Cell Biol *202*, 605-621.
931 Bembenek, J.N., Verbrugghe, K.J.C., Khanikar, J., Csankovszki, G., and Chan, R.C. (2013).
932 Condensin and the Spindle Midzone Prevent Cytokinesis Failure Induced by Chromatin
933 Bridges in C. elegans Embryos. Curr Biol *23*, 937-946.
934 Bembenek, J.N., White, J.G., and Zheng, Y.X. (2010). A Role for Separase in the Regulation
935 of RAB-11-Positive Vesicles at the Cleavage Furrow and Midbody. Curr Biol *20*, 259-264.
936 Bernabe-Rubio, M., Andres, G., Casares-Arias, J., Fernandez-Barrera, J., Rangel, L., Reglero-
937 Real, N., Gershlick, D.C., Fernandez, J.J., Millan, J., Correas, I.*, et al.* (2016). Novel role for
938 the midbody in primary ciliogenesis by polarized epithelial cells. J Cell Biol *214*, 259-273.
939 Bringmann, H., and Hyman, A.A. (2005). A cytokinesis furrow is positioned by two
940 consecutive signals. Nature *436*, 731-734.
941 Canman, J.C., Hoffman, D.B., and Salmon, E.D. (2000). The role of pre- and post-anaphase
942 microtubules in the cytokinesis phase of the cell cycle. Curr Biol *10*, 611-614.
943 Carlton, J.G., Caballe, A., Agromayor, M., Kloc, M., and Martin-Serrano, J. (2012). ESCRT-
944 III Governs the Aurora B-Mediated Abscission Checkpoint Through CHMP4C. Science *336*,
945 220-225.
946 Carmena, M., Earnshaw, W.C., and Glover, D.M. (2015). The Dawn of Aurora Kinase
947 Research: From Fly Genetics to the Clinic. Front Cell Dev Biol *3*, 73.
948 Chen, B.C., Legant, W.R., Wang, K., Shao, L., Milkie, D.E., Davidson, M.W., Janetopoulos,
949 C., Wu, X.F.S., Hammer, J.A., Liu, Z.*, et al.* (2014). Lattice light-sheet microscopy: Imaging
950 molecules to embryos at high spatiotemporal resolution. Science *346*, 439-+.
951 Chen, C.T., Ettinger, A.W., Huttner, W.B., and Doxsey, S.J. (2013). Resurrecting remnants:
952 the lives of post-mitotic midbodies. Trends Cell Biol *23*, 118-128.
953 Chen, J., Castelvecchi, G.D., Li-Villarreal, N., Raught, B., Krezel, A.M., McNeill, H., and
954 Solnica-Krezel, L. (2018). Atypical Cadherin Dachsous1b Interacts with Ttc28 and Aurora B
955 to Control Microtubule Dynamics in Embryonic Cleavages. Dev Cell *45*, 376-391 e375.
956 Crowell, E.F., Gaffuri, A.L., Gayraud-Morel, B., Tajbakhsh, S., and Echard, A. (2014).
957 Engulfment of the midbody remnant after cytokinesis in mammalian cells. J Cell Sci *127*,
958 3840-3851.
959 Dammermann, A., Pemble, H., Mitchell, B.J., McLeod, I., Yates, J.R., Kintner, C., Desai,
960 A.B., and Oegema, K. (2009). The hydrolethalus syndrome protein HYLS-1 links core
961 centriole structure to cilia formation. Gene Dev *23*, 2046-2059.
962 Dubreuil, V., Marzesco, A.M., Corbeil, D., Huttner, W.B., and Wilsch-Brauninger, M. (2007).
963 Midbody and primary cilium of neural progenitors release extracellular membrane particles
964 enriched in the stem cell marker prominin-1. J Cell Biol *176*, 483-495.
965 Eggert, U.S., Mitchison, T.J., and Field, C.M. (2006). Animal cytokinesis: From parts list to
966 mechanisms. Annu Rev Biochem *75*, 543-566.

967 El Amine, N., Kechad, A., Jananji, S., and Hickson, G.R. (2013). Opposing actions of septins
968 and Sticky on Anillin promote the transition from contractile to midbody ring. J Cell Biol *203*,
969 487-504.
970 Ettinger, A.W., Wilsch-Brauninger, M., Marzesco, A.M., Bickle, M., Lohmann, A., Maliga,
971 Z., Karbanova, J., Corbeil, D., Hyman, A.A., and Huttner, W.B. (2011). Proliferating versus
972 differentiating stem and cancer cells exhibit distinct midbody-release behaviour. Nat
973 Commun *2*, 503.
974 Feldman, J.L., and Priess, J.R. (2012). A role for the centrosome and PAR-3 in the hand-off
975 of MTOC function during epithelial polarization. Curr Biol *22*, 575-582.
976 Ferreira, J.G., Pereira, A.J., Akhmanova, A., and Maiato, H. (2013). Aurora B spatially
977 regulates EB3 phosphorylation to coordinate daughter cell adhesion with cytokinesis. J Cell
978 Biol *201*, 709-724.
979 Floyd, S., Whiffin, N., Gavilan, M.P., Kutscheidt, S., De Luca, M., Marcozzi, C., Min, M.,
980 Watkins, J., Chung, K., Fackler, O.T.*, et al.* (2013). Spatiotemporal organization of Aurora-B
981 by APC/CCdh1 after mitosis coordinates cell spreading through FHOD1. J Cell Sci *126*,
982 2845-2856.
983 Fox, D.T., and Duronio, R.J. (2013). Endoreplication and polyploidy: insights into
984 development and disease. Development *140*, 3-12.
985 Goto, H., Yasui, Y., Kawajiri, A., Nigg, E.A., Terada, Y., Tatsuka, M., Nagata, K., and
986 Inagaki, M. (2003). Aurora-B regulates the cleavage furrow-specific vimentin
987 phosphorylation in the cytokinetic process. J Biol Chem *278*, 8526-8530.
988 Green, R.A., Mayers, J.R., Wang, S., Lewellyn, L., Desai, A., Audhya, A., and Oegema, K.
989 (2013). The midbody ring scaffolds the abscission machinery in the absence of midbody
990 microtubules. J Cell Biol *203*, 505-520.
991 Green, R.A., Paluch, E., and Oegema, K. (2012). Cytokinesis in Animal Cells. Annu Rev Cell
992 Dev Bi *28*, 29-+.
993 Greenbaum, M.P., Ma, L., and Matzuk, M.M. (2007). Conversion of midbodies into germ cell
994 intercellular bridges. Developmental Biology *305*, 389-396.
995 Guizetti, J., Schermelleh, L., Mantler, J., Maar, S., Poser, I., Leonhardt, H., Muller-Reichert,
996 T., and Gerlich, D.W. (2011). Cortical constriction during abscission involves helices of
997 ESCRT-III-dependent filaments. Science *331*, 1616-1620.
998 Gwee, S.S.L., Radford, R.A.W., Chow, S., Syal, M.D., Morsch, M., Formella, I., Lee, A.,
999 Don, E.K., Badrock, A.P., Cole, N.J.*, et al.* (2018). Aurora kinase B regulates axonal
1000 outgrowth and regeneration in the spinal motor neurons of developing zebrafish. Cell Mol
1001 Life Sci.
1002 Haglund, K., Nezis, I.P., and Stenmark, H. (2011). Structure and functions of stable
1003 intercellular bridges formed by incomplete cytokinesis during development. Commun Integr
1004 Biol *4*, 1-9.
1005 Hardin, J., King, R., Thomas-Virnig, C., and Raich, W.B. (2008). Zygotic loss of ZEN-
1006 4/MKLP1 results in disruption of epidermal morphogenesis in the C. elegans embryo. Dev
1007 Dyn *237*, 830-836.
1008 Hedgecock, E.M., and White, J.G. (1985). Polyploid Tissues in the Nematode
1009 Caenorhabditis-Elegans. Developmental Biology *107*, 128-133.
1010 Heiman, M.G., and Shaham, S. (2009). DEX-1 and DYF-7 establish sensory dendrite length
1011 by anchoring dendritic tips during cell migration. Cell *137*, 344-355.
1012 Herszterg, S., Leibfried, A., Bosveld, F., Martin, C., and Bellaiche, Y. (2013). Interplay
1013 between the Dividing Cell and Its Neighbors Regulates Adherens Junction Formation during
1014 Cytokinesis in Epithelial Tissue. Dev Cell *24*, 256-270.
1015 Herszterg, S., Pinheiro, D., and Bellaiche, Y. (2014). A multicellular view of cytokinesis in
1016 epithelial tissue. Trends Cell Biol *24*, 285-293.
1017 Hime, G.R., Brill, J.A., and Fuller, M.T. (1996). Assembly of ring canals in the male germ
1018 line from structural components of the contractile ring. Journal of Cell Science *109*, 2779-
1019 2788.
1020 Hu, C.K., Coughlin, M., and Mitchison, T.J. (2012). Midbody assembly and its regulation
1021 during cytokinesis. Mol Biol Cell *23*, 1024-1034.

1022 Jordan, S.N., and Canman, J.C. (2012). Rho GTPases in Animal Cell Cytokinesis: An
1023 Occupation by the One Percent. Cytoskeleton *69*, 919-930.
1024 Kettenbach, A.N., Schweppe, D.K., Faherty, B.K., Pechenick, D., Pletnev, A.A., and Gerber,
1025 S.A. (2011). Quantitative Phosphoproteomics Identifies Substrates and Functional Modules of
1026 Aurora and Polo-Like Kinase Activities in Mitotic Cells. Sci Signal *4*.
1027 Kieserman, E.K., Glotzer, M., and Wallingford, J.B. (2008). Developmental regulation of
1028 central spindle assembly and cytokinesis during vertebrate embryogenesis. Curr Biol *18*, 116-
1029 123.
1030 Konig, J., Frankel, E.B., Audhya, A., and Muller-Reichert, T. (2017). Membrane remodeling
1031 during embryonic abscission in Caenorhabditis elegans. J Cell Biol.
1032 Lacroix, B., and Maddox, A.S. (2012). Cytokinesis, ploidy and aneuploidy. J Pathol *226*, 338-
1033 351.
1034 Leung, B., Hermann, G.J., and Priess, J.R. (1999). Organogenesis of the Caenorhabditis
1035 elegans intestine. Dev Biol *216*, 114-134.
1036 Li, D.Y., Mangan, A., Cicchini, L., Margolis, B., and Prekeris, R. (2014). FIP5
1037 phosphorylation during mitosis regulates apical trafficking and lumenogenesis. Embo Rep *15*,
1038 428-437.
1039 Li, R. (2007). Cytokinesis in development and disease: variations on a common theme. Cell
1040 Mol Life Sci *64*, 3044-3058.
1041 Linkert, M., Rueden, C.T., Allan, C., Burel, J.M., Moore, W., Patterson, A., Loranger, B.,
1042 Moore, J., Neves, C., MacDonald, D.*, et al.* (2010). Metadata matters: access to image data in
1043 the real world. J Cell Biol *189*, 777-782.
1044 Lujan, P., Varsano, G., Rubio, T., Hennrich, M.L., Sachsenheimer, T., Galvez-Santisteban,
1045 M., Martin-Belmonte, F., Gavin, A.C., Brugger, B., and Kohn, M. (2016). Phosphatase of
1046 regenerating liver (PRL)-3 disrupts epithelial architecture by altering the post-mitotic
1047 midbody position. J Cell Sci.
1048 Maddox, A.S., Habermann, B., Desai, A., and Oegema, K. (2005). Distinct roles for two C-
1049 elegans anillins in the gonad and early embryo. Development *132*, 2837-2848.
1050 Maddox, A.S., Lewellyn, L., Desai, A., and Oegema, K. (2007). Anillin and the septins
1051 promote asymmetric ingression of the cytokinetic furrow. Dev Cell *12*, 827-835.
1052 Mathieu, J., Cauvin, C., Moch, C., Radford, S.J., Sampaio, P., Perdigoto, C.N., Schweisguth,
1053 F., Bardin, A.J., Sunkel, C.E., Mckim, K.*, et al.* (2013). Aurora B and Cyclin B Have
1054 Opposite Effects on the Timing of Cytokinesis Abscission in Drosophila Germ Cells and in
1055 Vertebrate Somatic Cells. Dev Cell *26*, 250-265.
1056 McLachlan, I.G., and Heiman, M.G. (2013). Shaping dendrites with machinery borrowed
1057 from epithelia. Curr Opin Neurobiol *23*, 1005-1010.
1058 McLean, P.F., and Cooley, L. (2013). Protein Equilibration Through Somatic Ring Canals in
1059 Drosophila. Science *340*, 1445-1447.
1060 Morais-de-Sa, E., and Sunkel, C. (2013). Adherens junctions determine the apical position of
1061 the midbody during follicular epithelial cell division. Embo Rep *14*, 696-703.
1062 Nechipurenko, I.V., Berciu, C., Sengupta, P., and Nicastro, D. (2017). Centriolar remodeling
1063 underlies basal body maturation during ciliogenesis in Caenorhabditis elegans. eLife *6*.
1064 Norden, C., Mendoza, M., Dobbelaere, J., Kotwaliwale, C.V., Biggins, S., and Barral, Y.
1065 (2006). The NoCut pathway links completion of cytokinesis to spindle midzone function to
1066 prevent chromosome breakage. Cell *125*, 85-98.
1067 Oegema, K., and Hyman, A.A. (2006). Cell division. WormBook : the online review of C
1068 elegans biology, 1-40.
1069 Ou, G., Stuurman, N., D'Ambrosio, M., and Vale, R.D. (2010). Polarized myosin produces
1070 unequal-size daughters during asymmetric cell division. Science *330*, 677-680.
1071 Ou, G.S., Gentili, C., and Gonczy, P. (2014). Stereotyped distribution of midbody remnants in
1072 early C. elegans embryos requires cell death genes and is dispensable for development. Cell
1073 Res *24*, 251-253.
1074 Padmanabhan, A., and Zaidel-Bar, R. (2017). Non-junctional E-Cadherin Clusters Regulate
1075 the Actomyosin Cortex in the C. elegans Zygote. Mech Develop *145*, S85-S85.

1076 Paolini, A., Duchemin, A.L., Albadri, S., Patzel, E., Bornhorst, D., Avalos, P.G., Lemke, S.,
1077 Machate, A., Brand, M., Sel, S., *et al.* (2015). Asymmetric inheritance of the apical domain
1078 and self-renewal of retinal ganglion cell progenitors depend on Anillin function. Development
1079 *142*, 832-839.
1080 Perkins, L.A., Hedgecock, E.M., Thomson, J.N., and Culotti, J.G. (1986). Mutant Sensory
1081 Cilia in the Nematode Caenorhabditis-Elegans. Developmental Biology *117*, 456-487.
1082 Pohl, C., and Bao, Z. (2010). Chiral forces organize left-right patterning in C. elegans by
1083 uncoupling midline and anteroposterior axis. Dev Cell *19*, 402-412.
1084 Pollarolo, G., Schulz, J.G., Munck, S., and Dotti, C.G. (2011). Cytokinesis remnants define
1085 first neuronal asymmetry in vivo. Nat Neurosci *14*, 1525-1533.
1086 Portereiko, M.F., Saam, J., and Mango, S.E. (2004). ZEN-4/MKLP1 is required to polarize
1087 the foregut epithelium. Curr Biol *14*, 932-941.
1088 Rasmussen, J.P., Feldman, J.L., Reddy, S.S., and Priess, J.R. (2013). Cell Interactions and
1089 Patterned Intercalations Shape and Link Epithelial Tubes in C. elegans. Plos Genetics *9*.
1090 Rasmussen, J.P., Reddy, S.S., and Priess, J.R. (2012). Laminin is required to orient epithelial
1091 polarity in the C. elegans pharynx. Development *139*, 2050-2060.
1092 Reinsch, S., and Karsenti, E. (1994). Orientation of Spindle Axis and Distribution of Plasma-
1093 Membrane Proteins during Cell-Division in Polarized Mdckii Cells. J Cell Biol *126*, 1509-
1094 1526.
1095 Salzmann, V., Chen, C., Chiang, C.Y., Tiyaboonchai, A., Mayer, M., and Yamashita, Y.M.
1096 (2014). Centrosome-dependent asymmetric inheritance of the midbody ring in Drosophila
1097 germline stem cell division. Mol Biol Cell *25*, 267-275.
1098 Sato, K., Norris, A., Sato, M., and Grant, B.D. (2014). C. elegans as a model for membrane
1099 traffic. WormBook : the online review of C elegans biology, 1-47.
1100 Schiel, J.A., Childs, C., and Prekeris, R. (2013). Endocytic transport and cytokinesis: from
1101 regulation of the cytoskeleton to midbody inheritance. Trends Cell Biol *23*, 319-327.
1102 Schiel, J.A., Park, K., Morphew, M.K., Reid, E., Hoenger, A., and Prekeris, R. (2011).
1103 Endocytic membrane fusion and buckling-induced microtubule severing mediate cell
1104 abscission. J Cell Sci *124*, 1411-1424.
1105 Schindelin, J., Arganda-Carreras, I., Frise, E., Kaynig, V., Longair, M., Pietzsch, T., Preibisch,
1106 S., Rueden, C., Saalfeld, S., Schmid, B., *et al.* (2012). Fiji: an open-source platform for
1107 biological-image analysis. Nat Methods *9*, 676-682.
1108 Schluter, M.A., Pfarr, C.S., Pieczynski, J., Whiteman, E.L., Hurd, T.W., Fan, S.L., Liu, C.J.,
1109 and Margolis, B. (2009). Trafficking of Crumbs3 during Cytokinesis Is Crucial for Lumen
1110 Formation. Mol Biol Cell *20*, 4652-4663.
1111 Schumacher, J.M., Golden, A., and Donovan, P.J. (1998). AIR-2: An Aurora/Ipl1-related
1112 protein kinase associated with chromosomes and midbody microtubules is required for polar
1113 body extrusion and cytokinesis in Caenorhabditis elegans embryos. J Cell Biol *143*, 1635-
1114 1646.
1115 Severson, A.F., Hamill, D.R., Carter, J.C., Schumacher, J., and Bowerman, B. (2000). The
1116 Aurora-related kinase AIR-2 recruits ZEN-4/CeMKLP1 to the mitotic spindle at metaphase
1117 and is required for cytokinesis. Curr Biol *10*, 1162-1171.
1118 Siller, K.H., and Doe, C.Q. (2009). Spindle orientation during asymmetric cell division. Nat
1119 Cell Biol *11*, 365-374.
1120 Singh, D., and Pohl, C. (2014). Coupling of Rotational Cortical Flow, Asymmetric Midbody
1121 Positioning, and Spindle Rotation Mediates Dorsoventral Axis Formation in C. elegans. Dev
1122 Cell *28*, 253-267.
1123 Skop, A.R., Liu, H., Yates, J., 3rd, Meyer, B.J., and Heald, R. (2004). Dissection of the
1124 mammalian midbody proteome reveals conserved cytokinesis mechanisms. Science *305*, 61-
1125 66.
1126 Smith, K.P., Kieserman, E.K., Wang, P.I., Basten, S.G., Giles, R.H., Marcotte, E.M., and
1127 Wallingford, J.B. (2011). A Role for Central Spindle Proteins in Cilia Structure and Function.
1128 Cytoskeleton *68*, 112-124.

1129 Steigemann, P., Wurzenberger, C., Schmitz, M.H.A., Held, M., Guizetti, J., Maar, S., and
1130 Gerlich, D.W. (2009). Aurora B-Mediated Abscission Checkpoint Protects against
1131 Tetraploidization. Cell *136*, 473-484.
1132 Sulston, J.E., Schierenberg, E., White, J.G., and Thomson, J.N. (1983). The embryonic cell
1133 lineage of the nematode Caenorhabditis elegans. Dev Biol *100*, 64-119.
1134 Tong, Y.G., and Burglin, T.R. (2010). Conditions for dye-filling of sensory neurons in
1135 Caenorhabditis elegans. J Neurosci Meth *188*, 58-61.
1136 van Furden, D., Johnson, K., Segbert, C., and Bossinger, O. (2004). The C-elegans ezrin-
1137 radixin-moesin protein ERM-1 is necessary for apical junction remodelling and tubulogenesis
1138 in the intestine. Developmental Biology *272*, 262-276.
1139 Von Stetina, S.E., Liang, J., Marnellos, G., and Mango, S.E. (2017). Temporal regulation of
1140 epithelium formation mediated by FoxA, MKLP1, MgcRacGAP, and PAR-6. Mol Biol Cell
1141 *28*, 2042-2065.
1142 Waddle, J.A., Cooper, J.A., and Waterston, R.H. (1994). Transient localized accumulation of
1143 actin in Caenorhabditis elegans blastomeres with oriented asymmetric divisions.
1144 Development *120*, 2317-2328.
1145 Wang, J., Silva, M., Haas, L.A., Morsci, N.S., Nguyen, K.C.Q., Hall, D.H., and Barr, M.M.
1146 (2014a). C-elegans Ciliated Sensory Neurons Release Extracellular Vesicles that Function in
1147 Animal Communication. Curr Biol *24*, 519-525.
1148 Wang, T., Yanger, K., Stanger, B.Z., Cassio, D., and Bi, E. (2014b). Cytokinesis defines a
1149 spatial landmark for hepatocyte polarization and apical lumen formation. Journal of Cell
1150 Science *127*, 2483-2492.
1151 Wilcock, A.C., Swedlow, J.R., and Storey, K.G. (2007). Mitotic spindle orientation
1152 distinguishes stem cell and terminal modes of neuron production in the early spinal cord.
1153 Development *134*, 1943-1954.
1154 Yang, R.Z., and Feldman, J.L. (2015). SPD-2/CEP192 and CDK Are Limiting for
1155 Microtubule-Organizing Center Function at the Centrosome. Curr Biol *25*, 1924-1931.
1156 Zenker, J., White, M.D., Templin, R.M., Parton, R.G., Thorn-Seshold, O., Bissiere, S., and
1157 Plachta, N. (2017). A microtubule-organizing center directing intracellular transport in the
1158 early mouse embryo. Science *357*, 925-+.

1159

1160 **SUPPLEMENT FIGURE LEGENDS**

1161 **Figure S1. Immunostaining of endogenous Aurora B kinase during embryo development.**

1162 Immunostaining of Aurora B kinase (green) with DAPI (magenta) in wild type embryos. In
1163 early embryos, AIR-2 is observed at the central spindle (A), midbody flank (arrowhead in B),
1164 and midbody remnants (arrowheads in C, D). (E-G) Polarized E16 wild type embryo shows
1165 localization at the apical surface of the intestine (E-G, rectangle). Staining of wild type bean
1166 stage embryos shows apical localization in the pharynx (H-J, dotted circle) and at the apical
1167 cluster of the amphid sensilla (K-M, arrowheads). Scale bar, 10 μm.

1168

1169 **Figure S2. Cytokinesis in the intestine epithelia**

1170 Cytokinesis in the E8-E16 division. (A-C) ZEN-4::GFP (magenta, TBB-1::mCherry in green)
1171 appears on midbodies (A, numbered 1-8) that migrate to the midline (B) and are quickly
1172 removed (C, rectangle box). (D) Single plane imaging tracking the movement of ZEN-4::GFP
1173 (magenta,TBB-1::mCherry in green) to the apical surface. (E) Midbody from Eala at the E8-
1174 E16 division migrates towards the midline but the AIR-2 signal diminishes (green,
1175 PH::mCherry in magenta). (F-H) The apical surface marker, PAR-6::mCherry (G, magenta in
1176 F), colocalizes with AIR-2::GFP (H, green in F) at the apical midline. (I) Image series
1177 showing the simultaneous movement of AIR-2::GFP (red arrowhead) on the midbody and γ-
1178 tubulin::GFP (white arrowheads) on centrosomes to the apical surface. (J-L) RAB-
1179 11::mCherry (green) and AIR-2::GFP (magenta) colocalize on midbodies (labeled as 1-8 in J)
1180 as they migrate to the midline (K) and persist well after polarization is complete (L, rectangle).
1181 (M-O) In the terminal E16-E20 division, AIR-2::GFP appears on four midbodies (labeled
1182 according to E16 mother cell identity) that move to the apical midline (N, O). Time shown in
1183 minutes: seconds. Scale bar, 10 μm.

1184

1185 **Figure S3. Midbody dynamics during divisions of the early E lineage**

1186 (A) Diagram of the E-E2 division. Dynamics of Aurora B (B) and NMY-2 (C) show
1187 formation of the midbody (arrowheads) and rapid internalization. A similar pattern is also
1188 observed during the E2-E4 divisions (D-F) and the E4-E8 divisions (G-I), demonstrating that
1189 the early embryo divisions of the E lineage are similar until morphogenesis and epithelial
1190 polarization. Scale bar, 10 μm.

1191

1192 **Figure S4. Furrow and midbody localization of α-catenin during cytokinesis in the E**
1193 **lineage divisions**

1194 (A) Diagram of the E-E2 division. HMP-1::GFP localizes to the furrow and membrane
1195 adjacent to the midbody during cytokinesis (arrowheads in B). Shortly after this, apical
1196 constriction promotes gastrulation of the gut cells into the core of the embryo. (C) Diagram of
1197 the E2-E4 division. HMP-1::GFP can be observed in the cortex of the dividing cells and
1198 localizes along the furrow membrane for a short time after cytokinesis (arrowheads, D). (E)
1199 Diagram of the E4-E8 divisions. (F) Arrowheads indicate accumulation of HMP-1::GFP near
1200 the midbody during cytokinesis. HMP-1::GFP does not accumulate at the midline until the
1201 end of the E8-E16 division. Scale bar, 10 μm.

1202

1203 **Figure S5. Cytokinesis mutants have disrupted intestinal and pharyngeal tubulogenesis**

1204 (A) ERM-1 stains the apical lumen of the gut and pharynx in embryos at the comma stage.
1205 Persistence of gut lumen defects are observed in (B) *air-2(or207)* and (C) *zen-4(or153)*
1206 embryos. (D) Color-coded max Z-projections of A-C. (E-G) Staining of multiple apical
1207 surface markers in WT embryos shows normal localization of (E) PAR-3, (F) DLG-1 and (G)
1208 IFB-2. In *air-2(or207)* mutants, apical surface markers localize to distorted and mispositioned
1209 lumens (H-J). Scale bar, 10 μm.

1210

1211 **Figure S6. Cytokinesis in Pharynx Precursor Cells**

1212 (A-E) Centralspindlin ZEN-4::GFP dynamics in PPC divisions. Midbody remnants labeled
1213 with ZEN-4::GFP migrate to the midline (arrowheads, C) and are rapidly internalized and
1214 degraded. (F-K) AIR-2::GFP (H, K, green in merge) colocalized with TBB-1::mCherry (G,
1215 magenta in merge) and partially colocalized with RAB-11::mCherry (J, magenta in merge) at
1216 the apical surface of the polarized pharynx (dotted circle). (L-N) AIR-2::GFP (N, green in
1217 merge) partially co-localized with PAR-6::mCherry (M, magenta in merge) at the apical
1218 surface of the pharyngeal bulb (dotted circle). (O-Q) The apical surface of the pharynx
1219 accumulates γ-tubulin::GFP (P, magenta in merge, microtubules in green). Scale bar, 10 μm.

1220

1221 **Figure S7. Midbody components label dendrites of sensilla neurons**

1222 Aurora B kinase (green) colocalizes with (A-C) RAB-11::mCherry (magenta) and (D-F)
1223 TBB-1::mCherry (magenta) at the apical cluster in forming sensilla neurons (red arrowheads).

1224 (G-I) γ-tubulin::GFP (H, magenta in merge) localizes at the apical cluster with microtubules
1225 (I, green in merge). (J-L) AIR-2::GFP (green) localizes along the dendrite extension (dashed
1226 line) and PAR-6::mCherry is observed at the tip of the extension (arrowhead), indicating it is
1227 the apical domain. (M-O) AIR-2::GFP (green) and TBA-1::mCherry (magenta) colocalize
1228 along the length of the extended dendrite (dashed line). Scale bar, 10 μm.

1229

1230

1231

1232

1233

1234 **SUPPLEMENT MOVIE LEGENDS**

1235

1236 **Video S1. Cytokinesis in the first two mitotic divisions**

1237 Cytokinesis in the first (top row) or second (bottom row) division in embryos expressing
1238 AIR-2::GFP (green, left, with H2B::mCherry and PH::mCherry in magenta) or NMY-2::GFP
1239 (green, right, with PH::mCherry in magenta). White arrowheads indicate first midbody that is
1240 internalized by AB and red arrowheads indicate the AB midbody, which is engulfed by EMS.
1241 Images are max Z projections of 15 central planes spaced 1µm apart taken every 90 seconds.
1242 Playback rate is 2 frames/second.

1243

1244 **Video S2. Lattice Light Sheet Imaging of Intestinal Cytokinesis**

1245 E8-E16 intestinal cell divisions imaged in embryos expressing AIR-2::GFP (green) with
1246 PH::mCherry (magenta) with lattice light sheet microscopy. Max intensity projection of 100
1247 z-planes spaced 0.3 µm apart, acquired every 85 seconds.

1248

1249 **Video S3. Cytokinesis in the intestine epithelia**

1250 E8-E16 intestinal cell division in embryos expressing AIR-2::GFP (green, left, PH::mCherry
1251 in magenta), NMY-2::GFP (green, middle, tubulin::mCherry in magenta) or ZEN-4::GFP
1252 (green, right, tubulin::mCherry in magenta). The midbodies (indicated by arrowheads) form
1253 and move toward the apical surface. ZEN-4::GFP and NMY-2::GFP rapidly disappear, while
1254 AIR-2::GFP persists at the apical midline. Maximum z projections of 10 planes spaced 1µm
1255 apart, taken every 60 seconds. Playback rate is 6 frames/second.

1256

1257 **Video S4. High temporal resolution of midbody dynamics in the intestine**

1258 Imaging Earp cell division with high temporal resolution in an embryo expressing AIR-
1259 2::GFP (green, PH::mCherry in magenta) shows the lengthening of the central spindle and
1260 midbody migration event. Single plane images were acquired every 10 seconds. Playback rate
1261 is 15 frames/second.

1262

1263

1264 **Video S5. Cytokinesis in E16 to E20 cell division**

1265 E16-E20 cell division in embryos expressing AIR-2::GFP (green) with PH::mCherry and
1266 H2B::mCherry (magenta). Max z projection of 15 z planes 1 μm apart that were acquired
1267 every 90 seconds. Playback rate is 6 frames/second.

1268

1269 **Video S6. Microtubule dynamics during E8-E16 in Aurora B mutants.**

1270 WT (top row) and *air-2(or207)* (bottom row) mutant embryos expressing TBB-1::GFP (green
1271 in merge, right movie) and PH::mCherry and H2B::mCherry (middle, magenta in merge).
1272 Spindle midzone microtubules in WT embryos move to the midline where microtubules
1273 accumulate. In Aurora B mutant embryos, spindle midzone microtubules are diminished and
1274 cells that fail cytokinesis (right pair of gut cells) delay microtubule accumulation compared
1275 with the cells that do not fail. Max z projection of 10-15 z planes 1 μm apart that were
1276 acquired every 60 seconds. Playback rate is 6 frames/second.

1277

1278 **Video S7. Aurora B regulates adhesion dynamics during E8-E16 epithelial polarization.**

1279 WT (top row) and *air-2(or207)* (bottom row) mutant embryos expressing HMP-1::GFP
1280 (green in merge, right movie) and TBB-1::mCherry (top middle, magenta in upper left merge)
1281 or PH::mCherry and H2B::mCherry (bottom middle, magenta in lower left merge). In WT,
1282 HMP-1::GFP accumulates at the furrow and midbody as it migrates to the apical surface
1283 where it accumulates during polarization. In Aurora B mutant embryos, HMP-1::GFP is
1284 reduced in the furrow and midbody and cells that fail cytokinesis (left pair of gut cells) delay
1285 adhesion accumulation at the midline. Max z projection of 10-15 z planes 1 μm apart that
1286 were acquired every 60 seconds. Playback rate is 6 frames/second.

1287

1288 **Video S8. Cytokinesis in the pharynx from ventral views.**

1289 Cell division in pharyngeal precursor cells in embryos expressing AIR-2::GFP (green, left,
1290 H2B::mCherry in magenta), ZEN-4::GFP (green, middle left, TBB-1::mCherry in magenta),
1291 HMP-1::GFP (green, middle right, TBB-1::mCherry in magenta) or NMY-2::GFP (green,
1292 right, TBB-1::mCherry in magenta). Midbodies (white arrowheads) migrate toward
1293 pharyngeal midline after forming centrally between daughter cell pairs. Max z projection of
1294 10-15 z planes 1 μm apart that were acquired every 90 seconds. Playback rate is 6
1295 frames/second.

1296

1297 **Video S9. Lattice light sheet imaging of pharyngeal precursor cell divisions**

1298 Cytokinesis in pharyngeal precursor cell divisions in embryos expressing AIR-2::GFP (green,
1299 PH::mCherry in magenta). Max intensity projection of 101 z-planes spaced 0.35 µm apart,
1300 acquired every 60 seconds. Playback rate is 7 frames/second.

1301

1302 **Video S10. Cytokinesis in the sensilla dendrite development**

1303 Cell division in sensilla precursor cell divisions in embryos expressing AIR-2::GFP (green,
1304 left, H2B::mCherry in magenta), ZEN-4::GFP (green, middle left, TBB-1::mCherry in
1305 magenta), NMY-2::GFP (green, middle right, TBB-1::mCherry in magenta), or HMP-1::GFP
1306 (green, right, TBB-1::mCherry in magenta). Midbodies (white arrowheads) migrate into an
1307 apical cluster. Max z projection of 10 z planes 1 µm apart that were acquired every 90
1308 seconds. Playback rate is 6 frames/second.

1309

1310 **Video S11. Lattice Light Sheet imaging of Sensilla Precursor Cell Division**

1311 Embryos expressing midbody flank marker AIR-2::GFP (green) with PH::mCherry (magenta)
1312 were imaged during the sensilla precursor divisions. Max intensity projection of 111 z-planes
1313 spaced 0.35 µm apart, acquired every 60 seconds. Playback rate is 7 frames/second.

1314

1315 **Video S12. Dendrite Extension of sensilla neurons**

1316 Embryo expressing AIR-2::GFP from the apical cluster stage of amphid polarization through
1317 the process of dendrite extension. Max z projection of 7 z planes 1 µm apart viewed from the
1318 ventral aspect and acquired every 90 seconds. Playback rate is 6 frames/second.

1319

1320

Figure 1

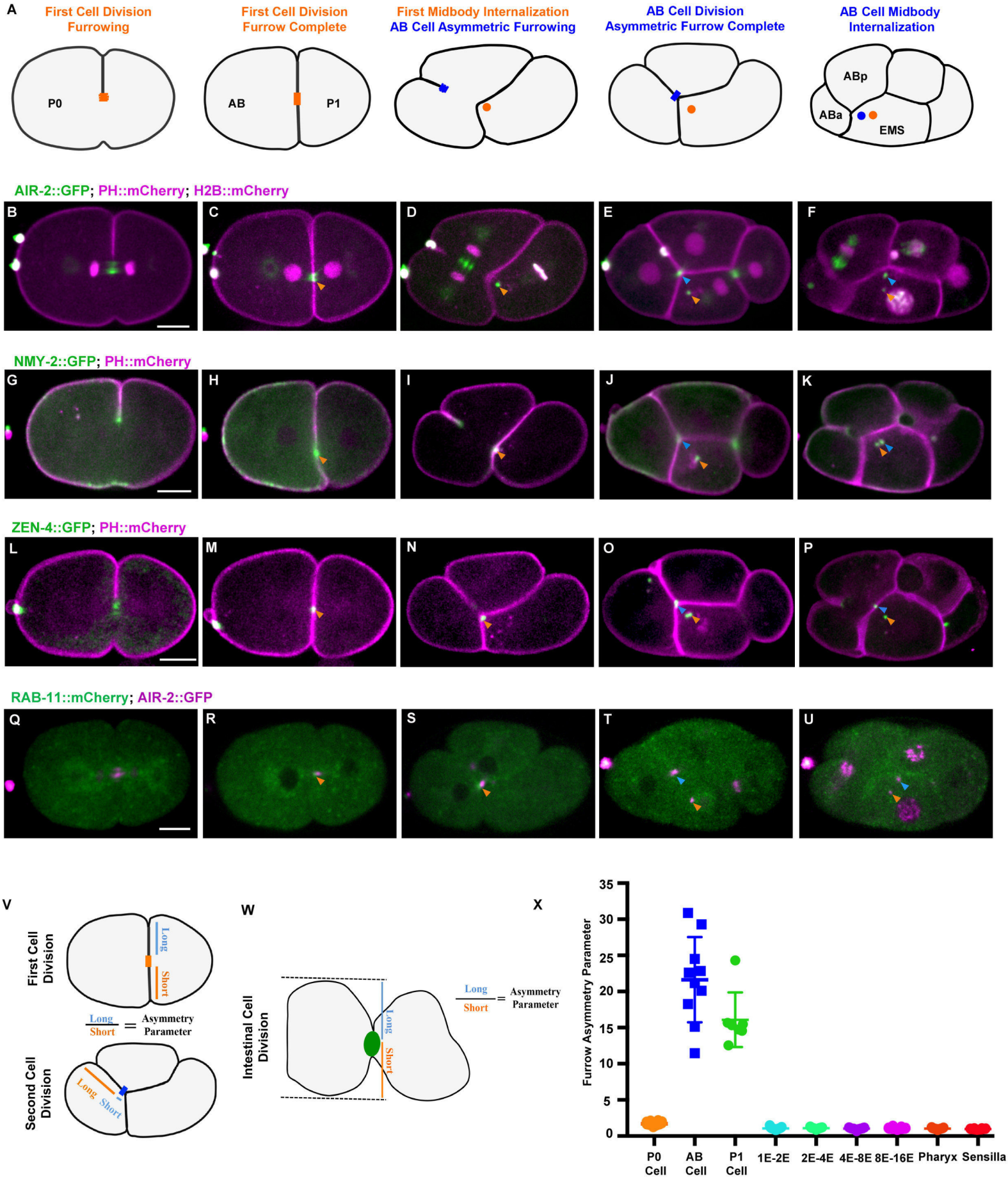
A
First Cell Division Furrowing
First Cell Division Furrow Complete
First Midbody Internalization AB Cell Asymmetric Furrowing
AB Cell Division Asymmetric Furrow Complete
AB Cell Midbody Internalization
P0
AB
P1
ABp
ABa
EMS
AIR-2::GFP; PH::mCherry; H2B::mCherry
B
C
D
E
F
NMY-2::GFP; PH::mCherry
G
H
I
J
K
ZEN-4::GFP; PH::mCherry
L
M
N
O
P
RAB-11::mCherry; AIR-2::GFP
Q
R
S
T
U
V
First Cell Division
Long
Short
Long / Short = Asymmetry Parameter
Second Cell Division
Long
Short
W
Intestinal Cell Division
Long
Short
Long / Short = Asymmetry Parameter
X
Furrow Asymmetry Parameter
35
30
25
20
15
10
5
0
P0 Cell
AB Cell
P1 Cell
1E-2E
2E-4E
4E-8E
8E-16E
Pharyx
Sensilla

Figure 2

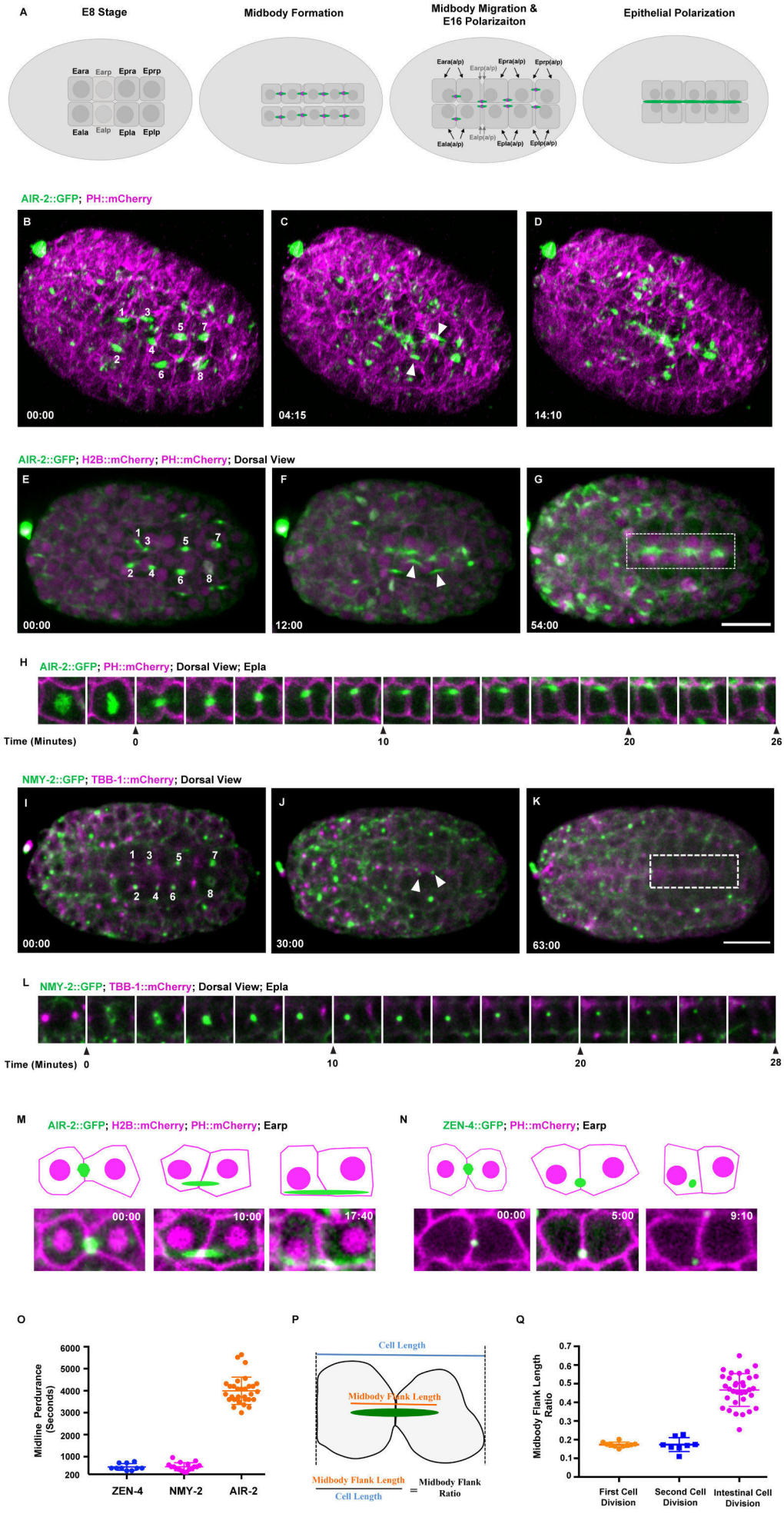
A
E8 Stage
Midbody Formation
Midbody Migration & E16 Polarizaiton
Epithelial Polarization
Eara
Earp
Epra
Eprp
Eala
Ealp
Epla
Eplp
AIR-2::GFP; PH::mCherry
B
C
D
00:00
04:15
14:10
AIR-2::GFP; H2B::mCherry; PH::mCherry; Dorsal View
E
F
G
00:00
12:00
54:00
H
AIR-2::GFP; PH::mCherry; Dorsal View; Epla
Time (Minutes)
0
10
20
26
NMY-2::GFP; TBB-1::mCherry; Dorsal View
I
J
K
00:00
30:00
63:00
L
NMY-2::GFP; TBB-1::mCherry; Dorsal View; Epla
Time (Minutes)
0
10
20
28
M
AIR-2::GFP; H2B::mCherry; PH::mCherry; Earp
00:00
10:00
17:40
N
ZEN-4::GFP; PH::mCherry; Earp
00:00
5:00
9:10
O
Midline Perdurance (Seconds)
ZEN-4
NMY-2
AIR-2
P
Cell Length
Midbody Flank Length
Midbody Flank Length / Cell Length = Midbody Flank Ratio
Q
Midbody Flank Length Ratio
First Cell Division
Second Cell Division
Intestinal Cell Division

Figure 3

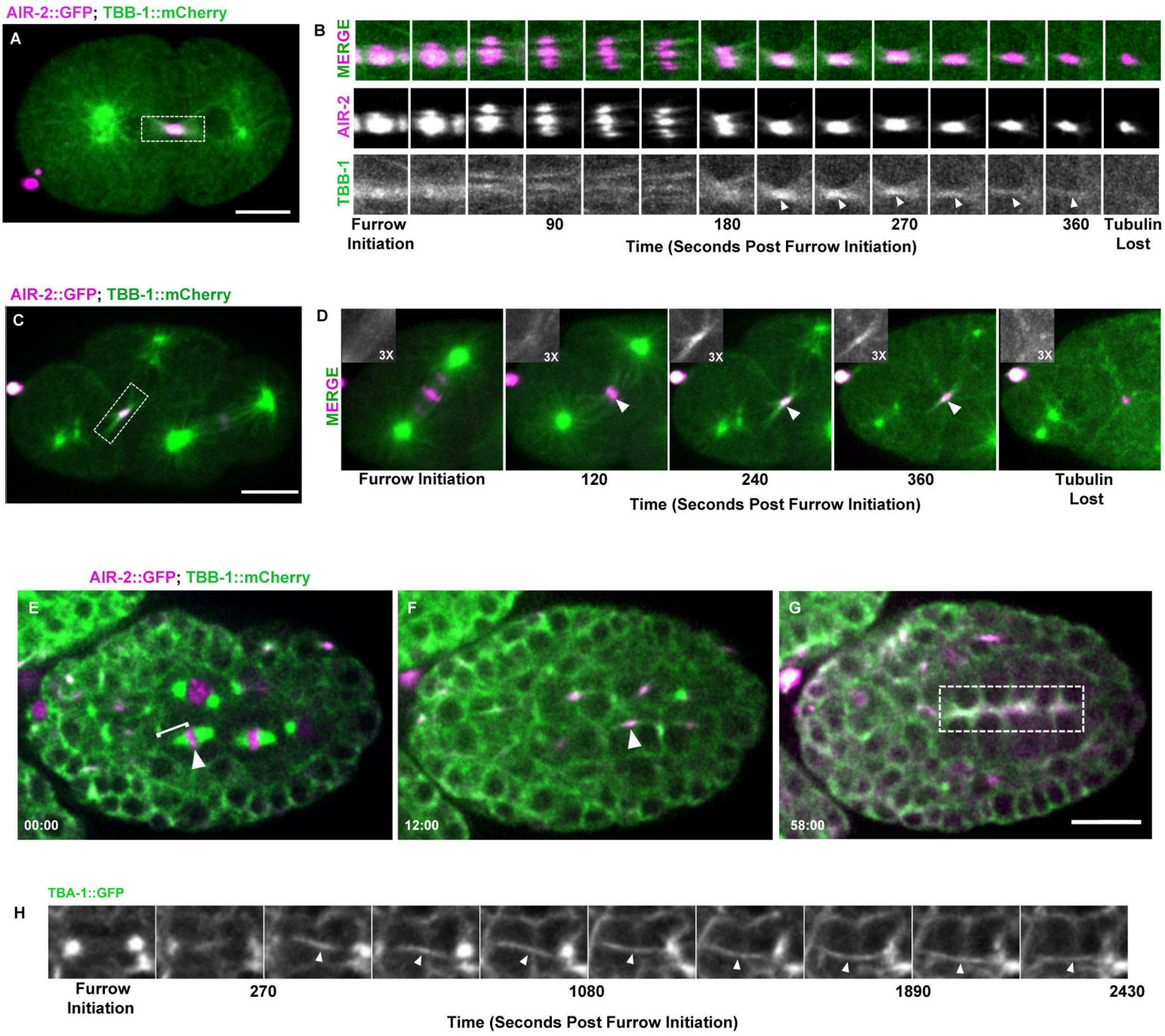
AIR-2::GFP; TBB-1::mCherry
A
B
MERGE
AIR-2
TBB-1
Furrow Initiation
90
180
270
360
Tubulin Lost
Time (Seconds Post Furrow Initiation)
AIR-2::GFP; TBB-1::mCherry
C
D
3X
MERGE
Furrow Initiation
120
240
360
Tubulin Lost
Time (Seconds Post Furrow Initiation)
AIR-2::GFP; TBB-1::mCherry
E
F
G
00:00
12:00
58:00
TBA-1::GFP
H
Furrow Initiation
270
1080
1890
2430
Time (Seconds Post Furrow Initiation)
I
Tubulin Disassemble Time (Seconds)
2000
1500
1000
500
0
P0 Cell
AB Cell
P1 Cell
1E-2E
2E-4E
4E-8E
8E-16E

Figure 4

A

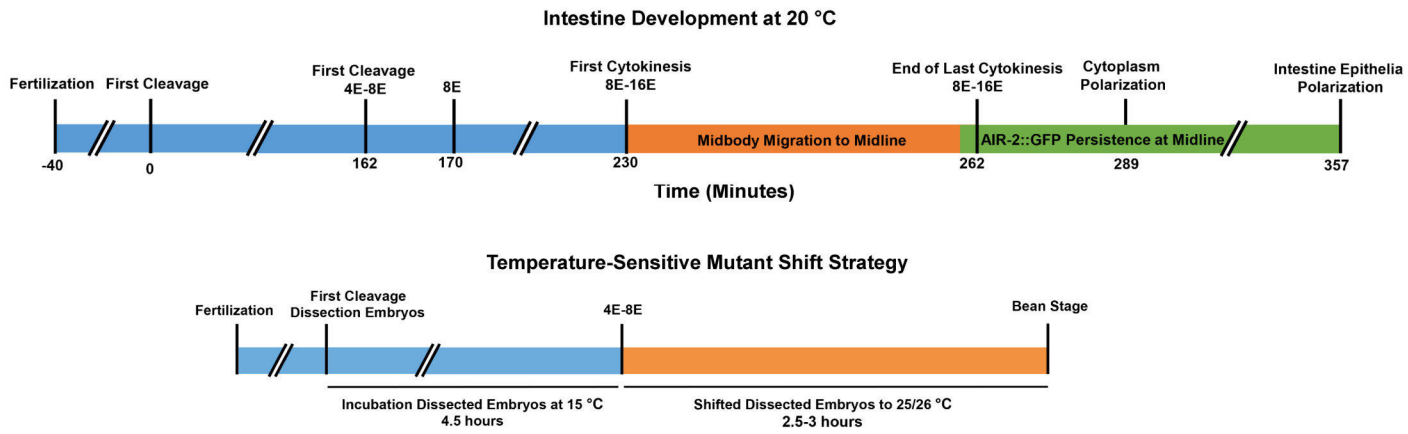

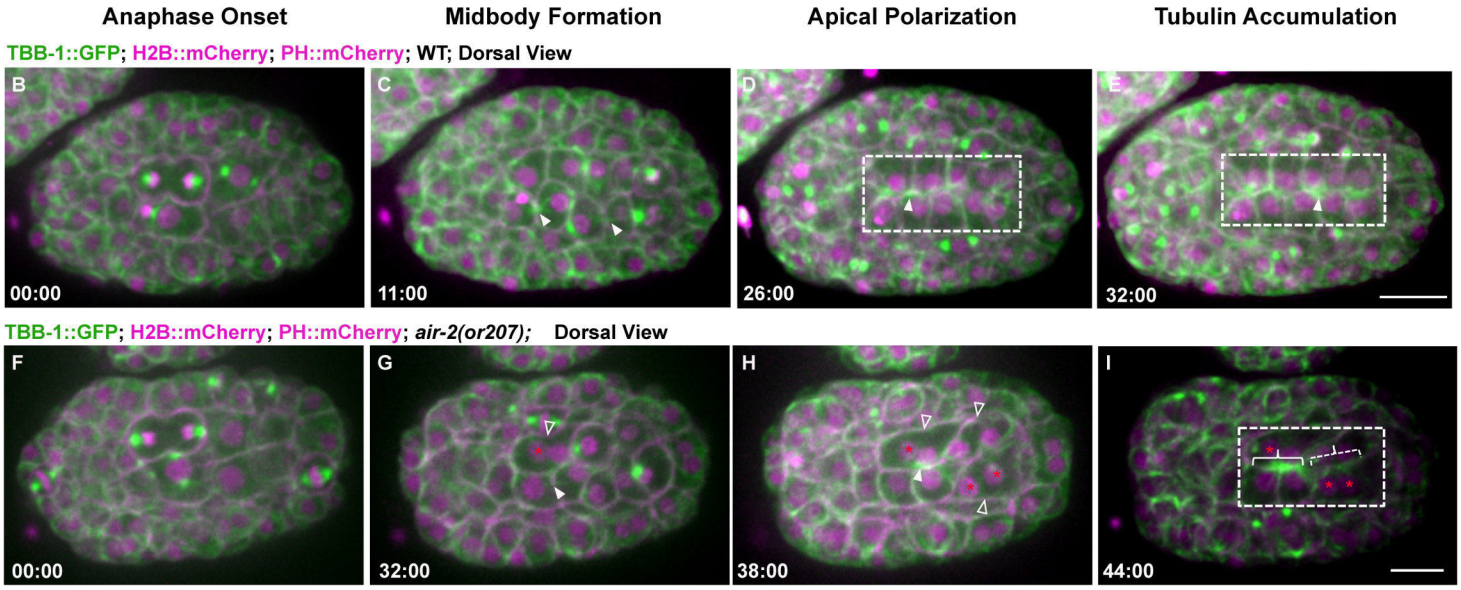

J

Genotype	Total Embryo	Total 8E Cells	Cytokinesis Failure	Nuclei Polarization Defects	Chromosome Segregation Defects	Microtubule Accumulation Defects
WT (N2)	8	34	0/34 (0%)	0/34 (0%)	0/34 (0%)	0/8 (0%)
air-2(or207)	11	66	18/66 (27.3%)	17/66 (25.8%)	3/66 (4.5%)	5/11 (45.5%)

K

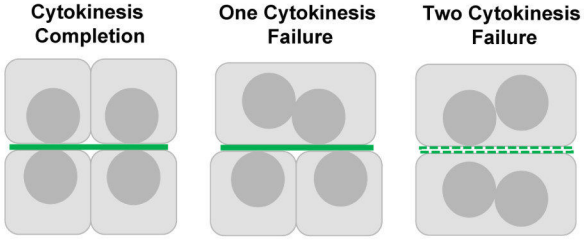

L

Genotype	Pair of 8E Cells	Pair Number	One Cytokinesis Failure	Microtubule Discontinuous	Two Cytokinesis Failure	Microtubule Discontinuous
WT (N2)	Ea(r/l)a	8	0/8 (0%)	0/0 (0%)	0/8 (0%)	0/0 (0%)
	Ea(r/l)p	8	0/8 (0%)	0/0 (0%)	0/8 (0%)	0/0 (0%)
	Ep(r/l)a	8	0/8 (0%)	0/0 (0%)	0/8 (0%)	0/0 (0%)
air-2(or207)	Ea(r/l)a	11	5/11 (45.5%)	1/5 (20%)	0/11 (0%)	0/0 (0%)
	Ea(r/l)p	11	6/11 (54.4%)	0/6 (0%)	0/11 (0%)	0/0 (0%)
	Ep(r/l)a	11	3/11 (27.3%)	1/3 (33.3%)	2/11 (18.2%)	1/2 (50.0%)

Figure 5

Anaphase Onset | Midbody Formation & Migration | Tubulin and Accumulation

HMP-1::GFP; TBB-1::mCherry; WT; Dorsal View

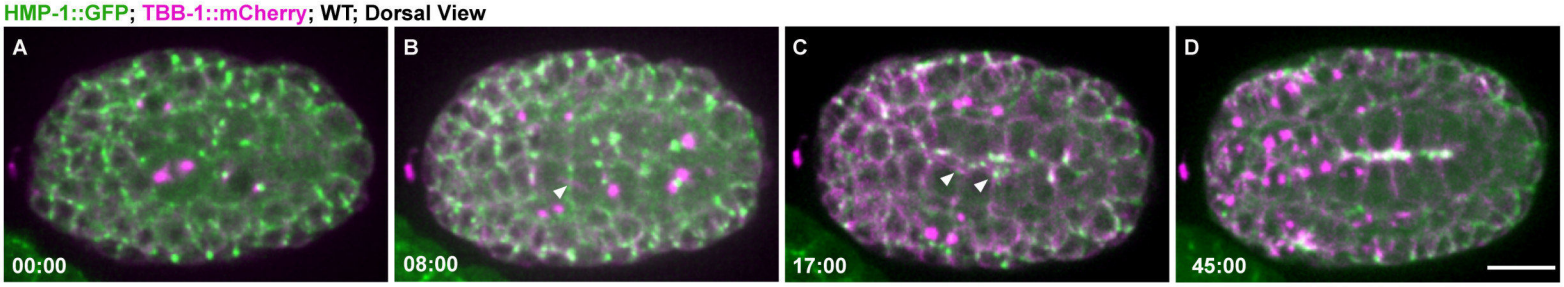

E HMP-1::GFP; TBB-1::mCherry; WT; Ealp; Dorsal View

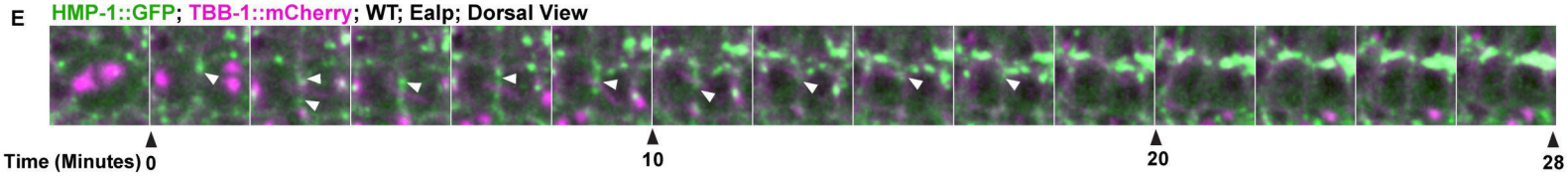

HMP-1::GFP; H2B::mCherry; PH::mCherry; *air-2(or207)*; Dorsal View

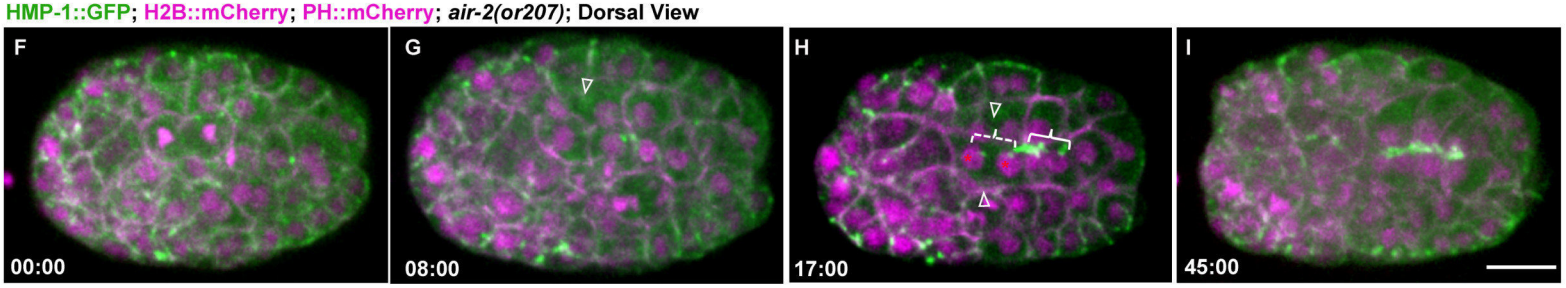

J HMP-1::GFP; H2B::mCherry; PH::mCherry; *air-2(or207)*; Dorsal View

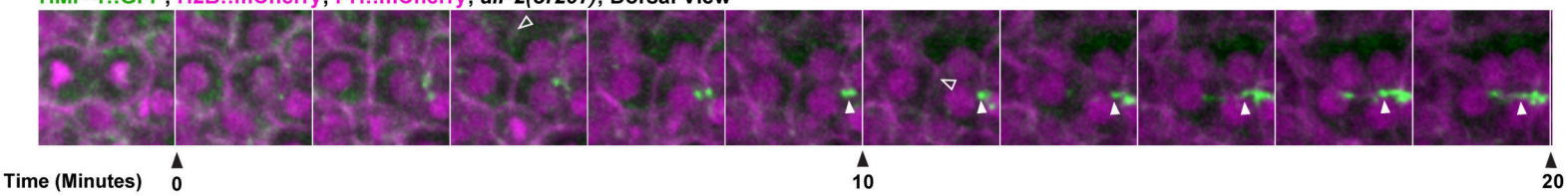

K

Genotype	Total Embryo	Total 8E Cells	Cytokinesis Failure	Nuclei Polarization Defects	Chromosome Segregation Defects	HMP-1 Accumulation Defects
WT (N2)	5	30	0/30 (0%)	0/30 (0%)	0/30 (0%)	0/5 (0%)
air-2(or207)	12	72	30/72 (41.7%)	25/72 (34.7%)	0/72 (0%)	6/12 (50.0%)

L

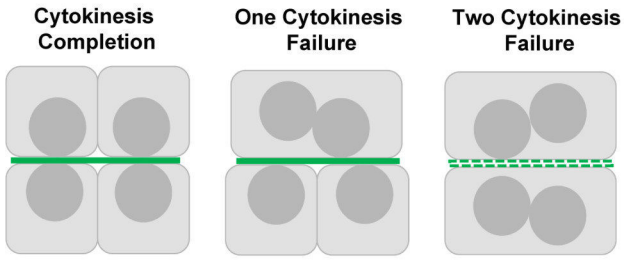

M

Genotype	Pair of 8E Cells	Pair Number	One Cytokinesis Failure	HMP-1 Discontinuous	Two Cytokinesis Failure	HMP-1 Discontinuous
WT (N2)	Ea(r/l)a	5	0/5 (0%)	0/0 (0%)	0/5 (0%)	0/0 (0%)
	Ea(r/l)p	5	0/5 (0%)	0/0 (0%)	0/5 (0%)	0/0 (0%)
	Ep(r/l)a	5	0/5 (0%)	0/0 (0%)	0/5 (0%)	0/0 (0%)
air-2(or207)	Ea(r/l)a	12	3/12 (45.5%)	0/3 (0%)	3/12 (0%)	3/3 (100%)
	Ea(r/l)p	12	6/12 (54.4%)	0/6 (0%)	1/12 (8.3%)	0/1 (0%)
	Ep(r/l)a	12	4/12 (33.3%)	0/4 (0%)	4/12 (33.3%)	3/4 (75.0%)

Figure 6

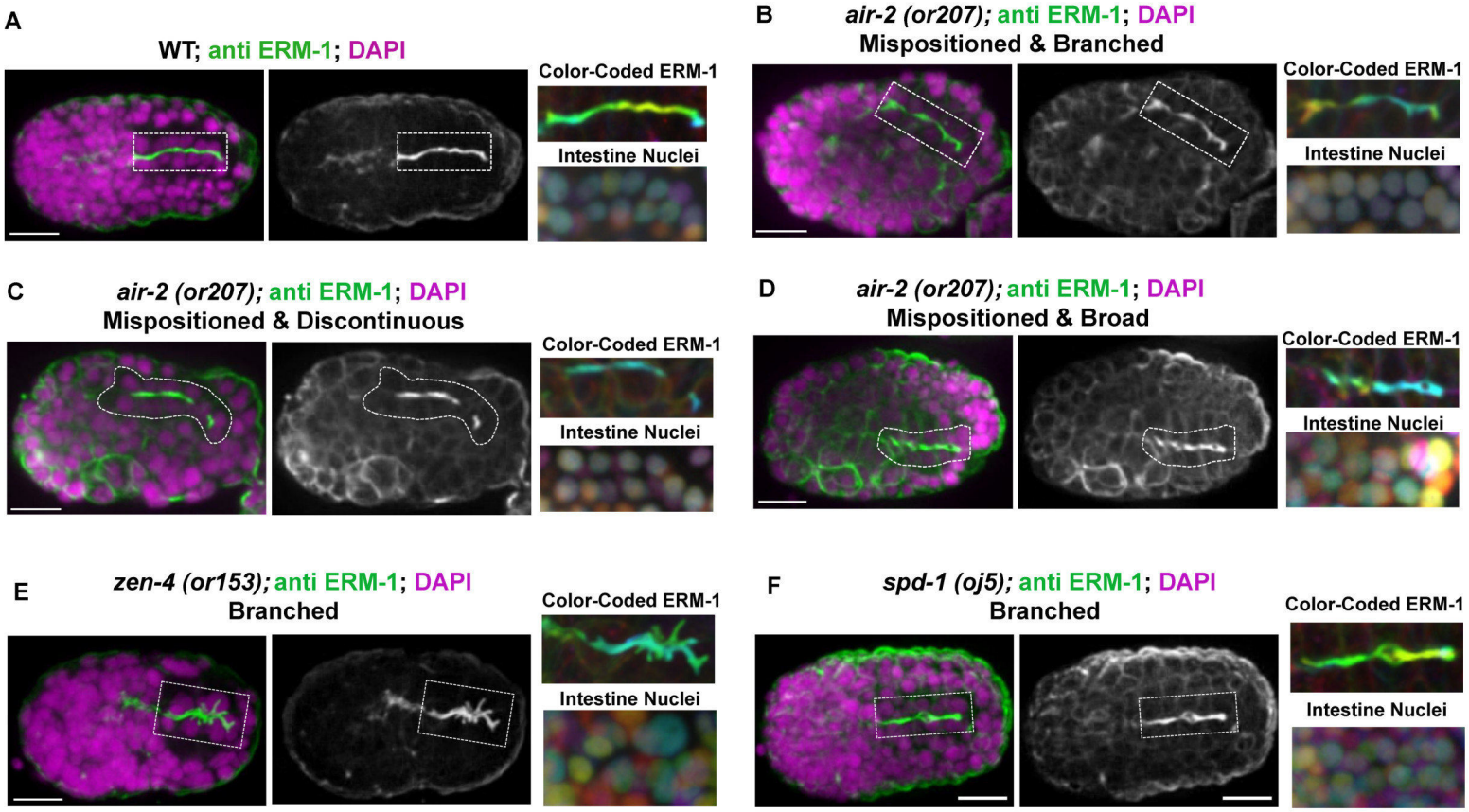

G

	Mispositioned	Discontinuous	Broad	Branched
WT (N2)	0% (0/60)	0% (0/60)	3.3% (2/60)	20% (12/60)
air-2 (or207)	60.9% (25/41)	43.9% (18/41)	12.1% (5/41)	65.9% (27/41)
zen-4 (or153)	27.3% (6/22)	27.3% (6/22)	81.8% (18/22)	81.8% (18/22)
spd-1 (oj5)	0% (0/59)	28.8% (17/59)	10.2% (6/59)	40% (24/59)

H

	One Color	Two Color	Three Color	Four Color	Five Color	Six Color
WT (N2)	25% (15/60)	40% (24/60)	31.7% (19/60)	3.3% (2/60)	0% (0/60)	0% (0/60)
air-2 (or207)	0% (0/41)	22.0% (9/41)	12.2% (9/41)	34.1% (14/41)	14.6% (6/41)	17.1% (7/41)
zen-4 (or153)	0% (0/22)	27.3% (6/22)	40.9% (9/22)	22.7% (5/22)	4.5% (1/22)	0% (0/22)
spd-1 (oj5)	10.2% (6/59)	55.9% (33/59)	27.1% (16/59)	1.7% (1/59)	1.7% (1/59)	0% (0/59)

Figure 7

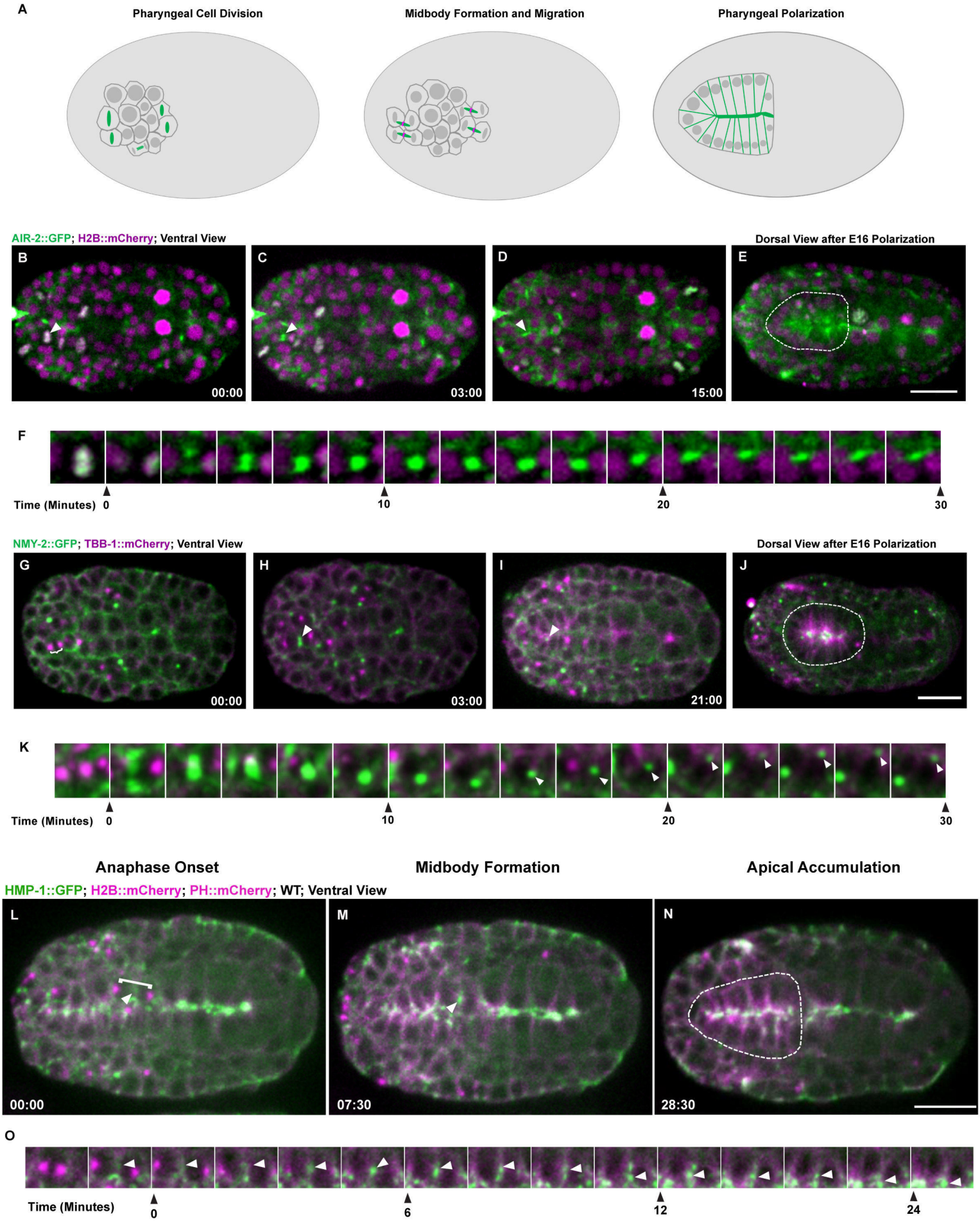
A
Pharyngeal Cell Division
Midbody Formation and Migration
Pharyngeal Polarization
AIR-2::GFP; H2B::mCherry; Ventral View
Dorsal View after E16 Polarization
B
C
D
E
00:00
03:00
15:00
F
Time (Minutes) 0
10
20
30
NMY-2::GFP; TBB-1::mCherry; Ventral View
Dorsal View after E16 Polarization
G
H
I
J
00:00
03:00
21:00
K
Time (Minutes) 0
10
20
30
Anaphase Onset
Midbody Formation
Apical Accumulation
HMP-1::GFP; H2B::mCherry; PH::mCherry; WT; Ventral View
L
M
N
00:00
07:30
28:30
O
Time (Minutes) 0
6
12
24

Figure 8

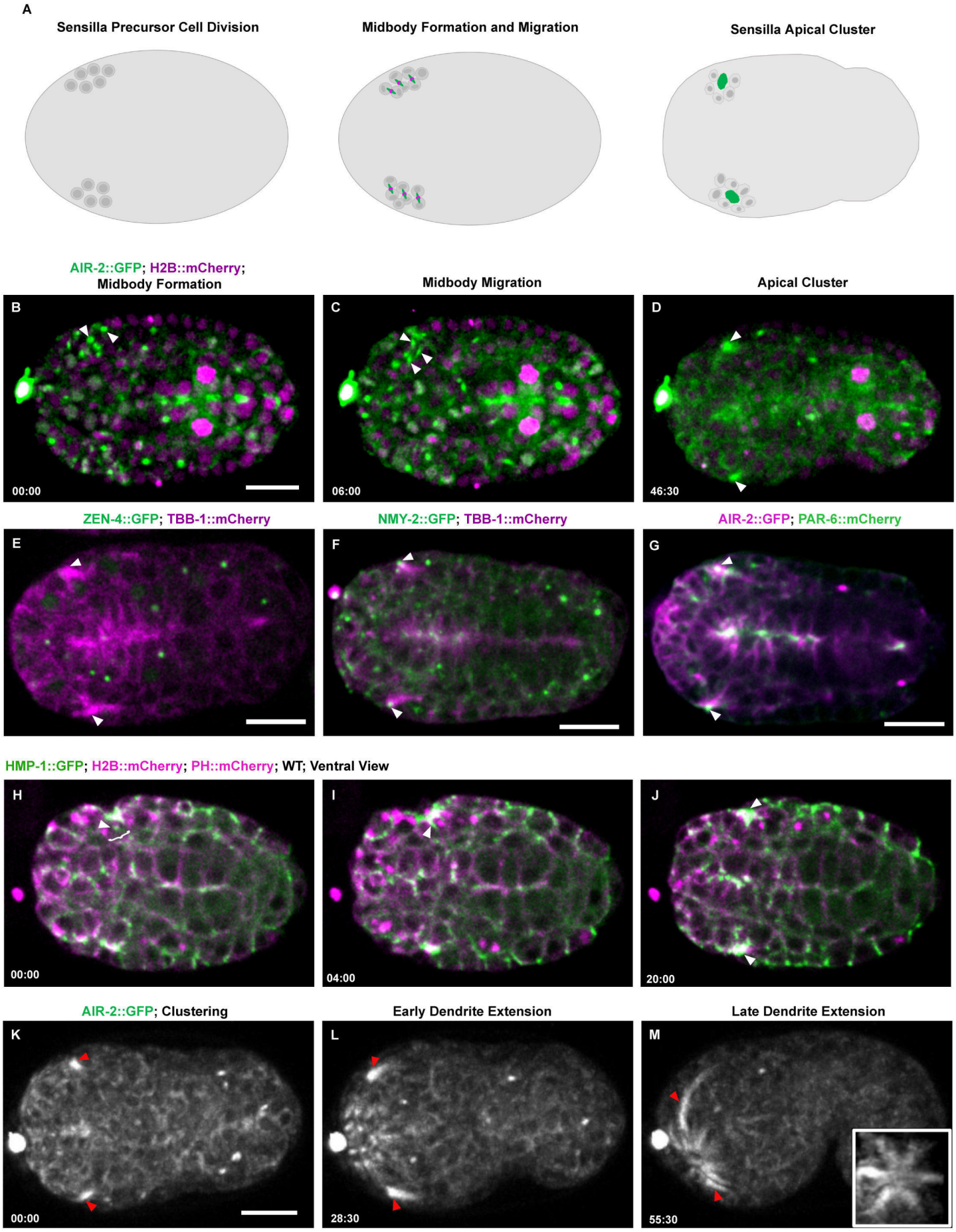
A
Sensilla Precursor Cell Division
Midbody Formation and Migration
Sensilla Apical Cluster
AIR-2::GFP; H2B::mCherry;
Midbody Formation
Midbody Migration
Apical Cluster
B
00:00
C
06:00
D
46:30
ZEN-4::GFP; TBB-1::mCherry
NMY-2::GFP; TBB-1::mCherry
AIR-2::GFP; PAR-6::mCherry
E
F
G
HMP-1::GFP; H2B::mCherry; PH::mCherry; WT; Ventral View
H
00:00
I
04:00
J
20:00
AIR-2::GFP; Clustering
Early Dendrite Extension
Late Dendrite Extension
K
00:00
L
28:30
M
55:30

Figure 9

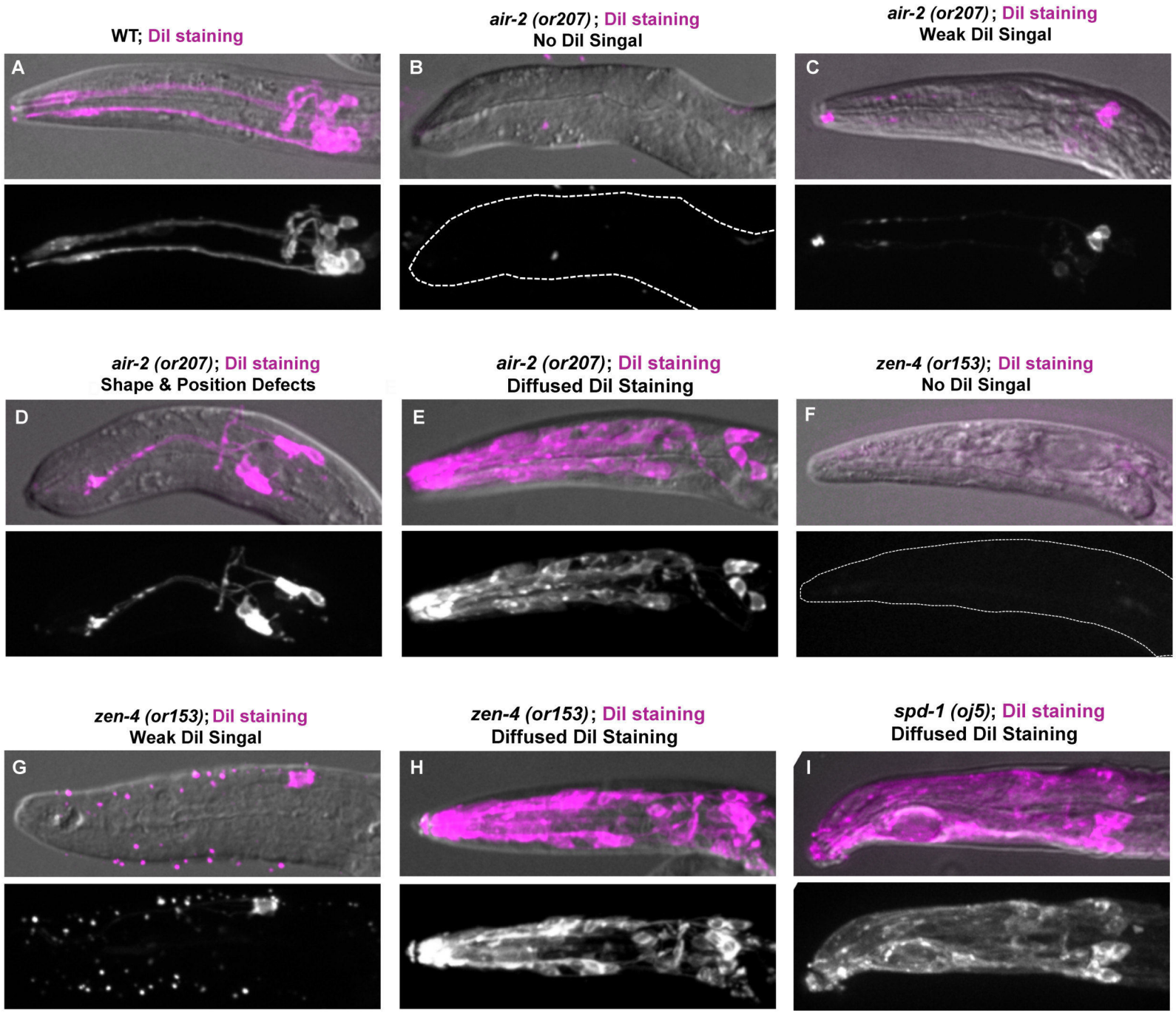
WT; Dil staining
A
air-2 (or207); Dil staining
No Dil Singal
B
air-2 (or207); Dil staining
Weak Dil Singal
C
air-2 (or207); Dil staining
Shape & Position Defects
D
air-2 (or207); Dil staining
Diffused Dil Staining
E
zen-4 (or153); Dil staining
No Dil Singal
F
zen-4 (or153); Dil staining
Weak Dil Singal
G
zen-4 (or153); Dil staining
Diffused Dil Staining
H
spd-1 (oj5); Dil staining
Diffused Dil Staining
I

Supplement Figure 1

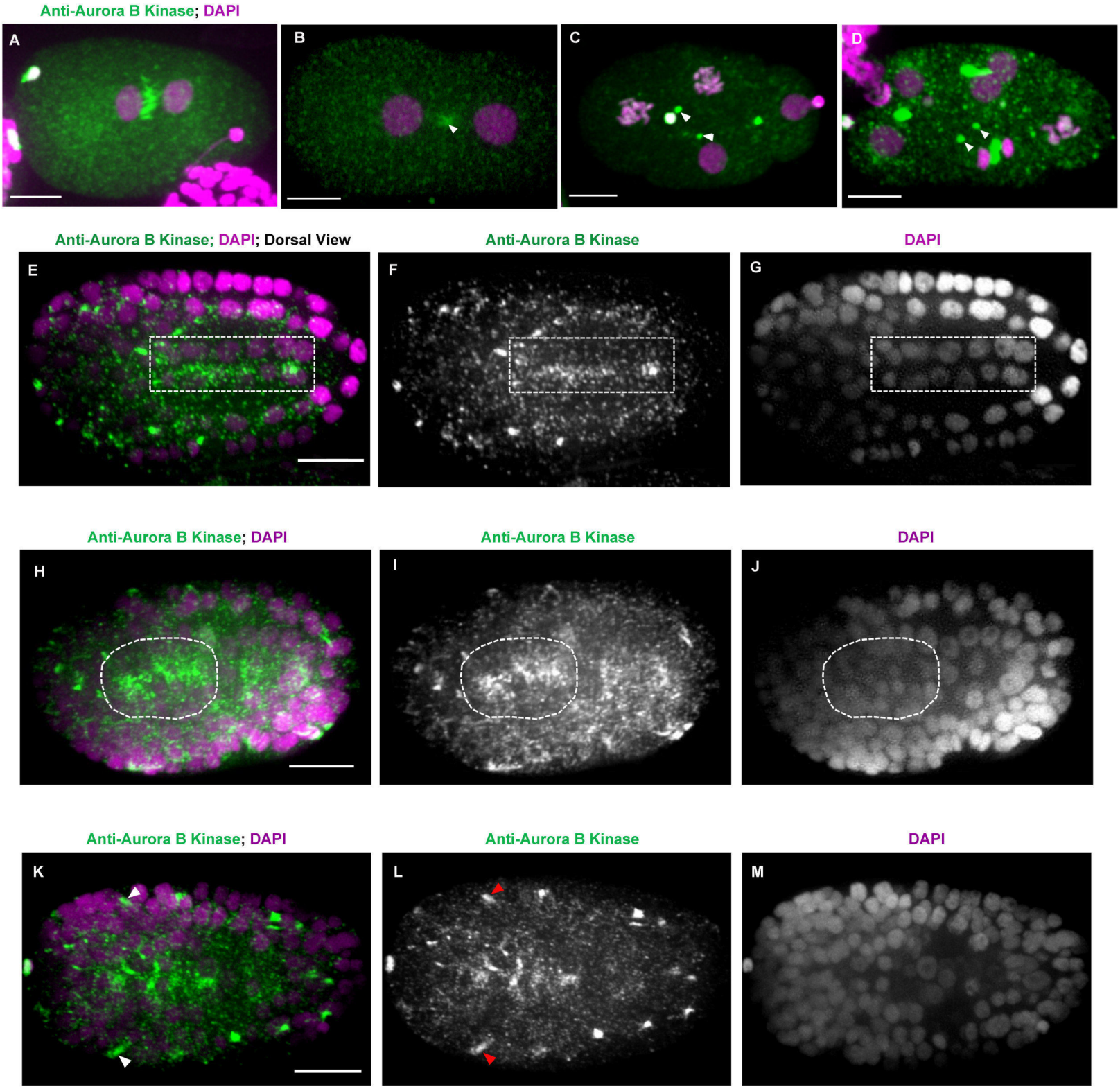

Supplement Figure 2

ZEN-4::GFP; TBB-1::mCherry

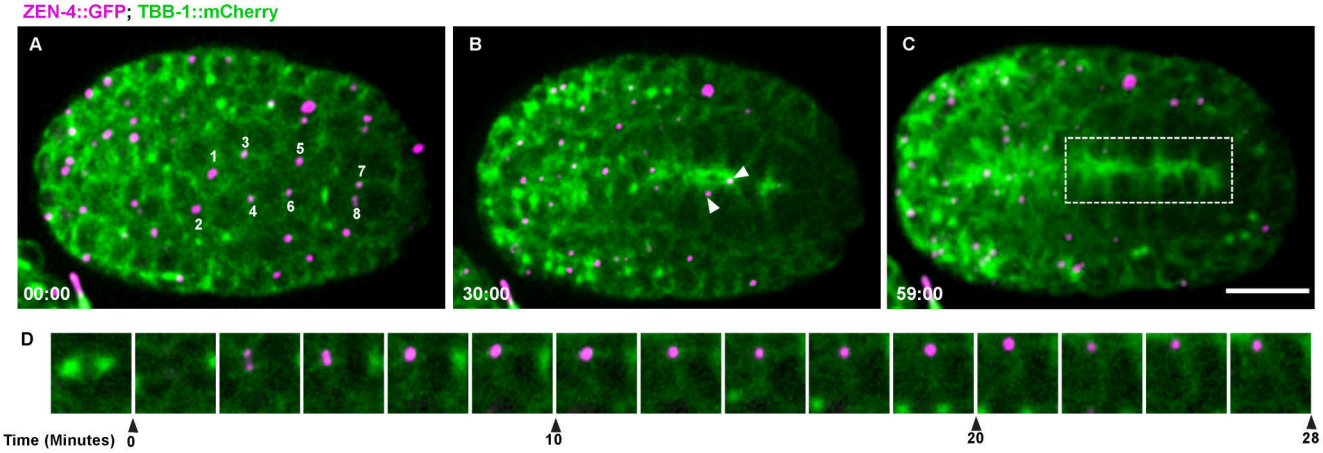

E AIR-2::GFP; PH::mCherry; Dorsal View; Eala

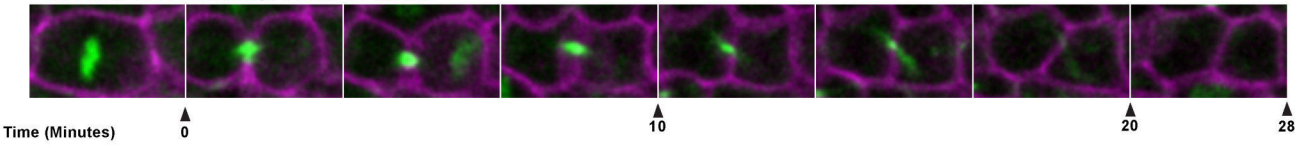

AIR-2::GFP; PAR-6::mCherry; Dorsal View

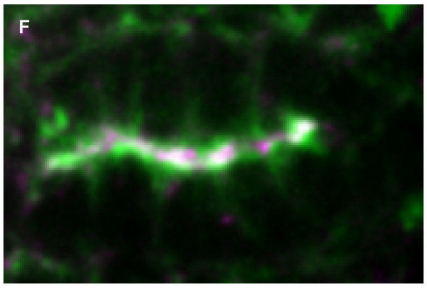

PAR-6::mCherry

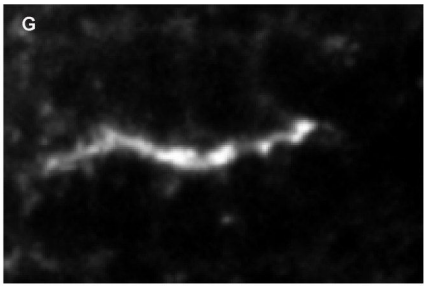

AIR-2::GFP

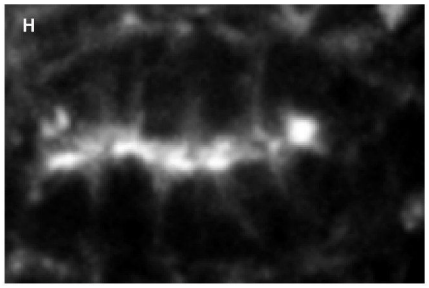

I γ-Tublin::GFP; AIR-2::GFP; Dorsal View; Epla

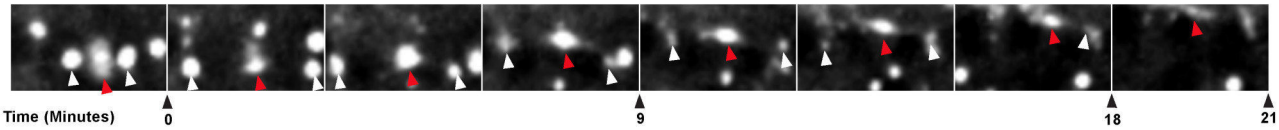

RAB-11::mCherry; AIR-2::GFP; Dorsal View

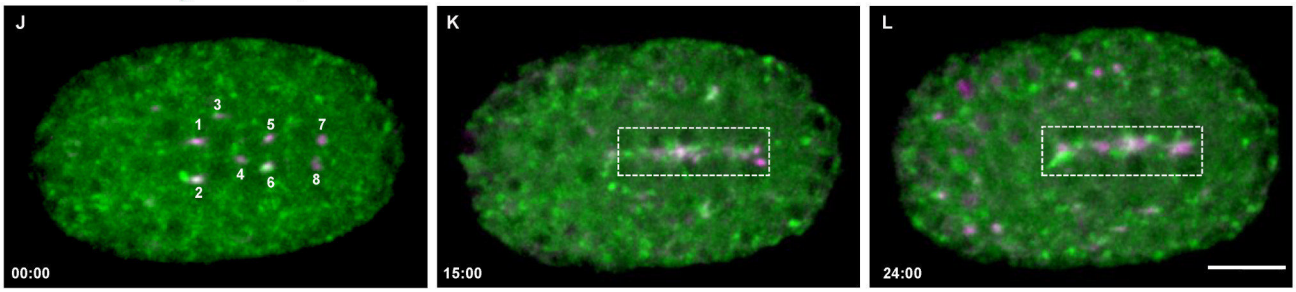

AIR-2::GFP; H2B::mCherry; Dorsal View

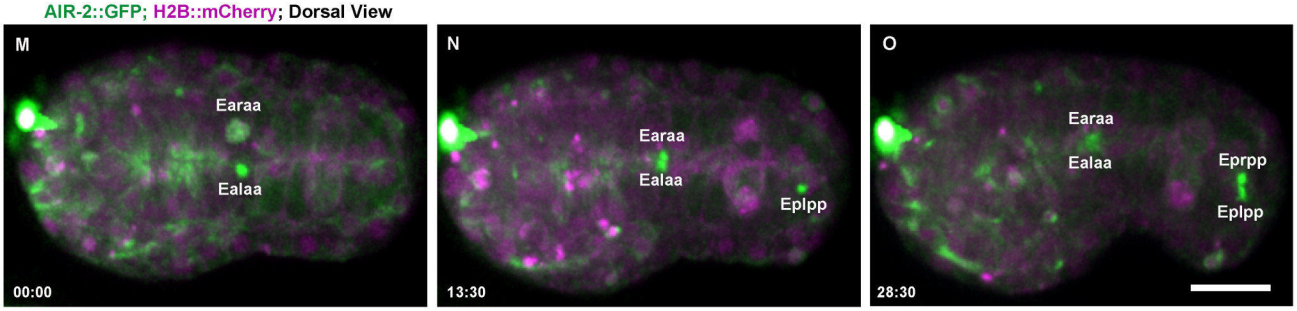

Supplement Figure 3

A

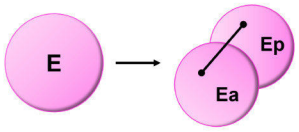

AIR-2::GFP; H2B::mCherry; PH::mCherry; 1E-2E

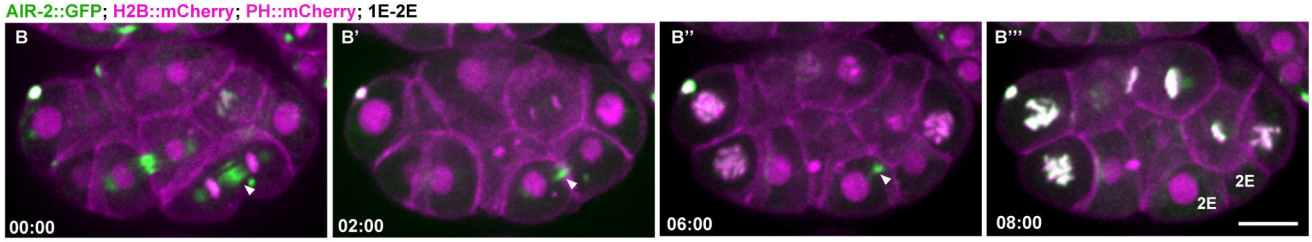

NMY-2::GFP; PH::mCherry; 1E-2E

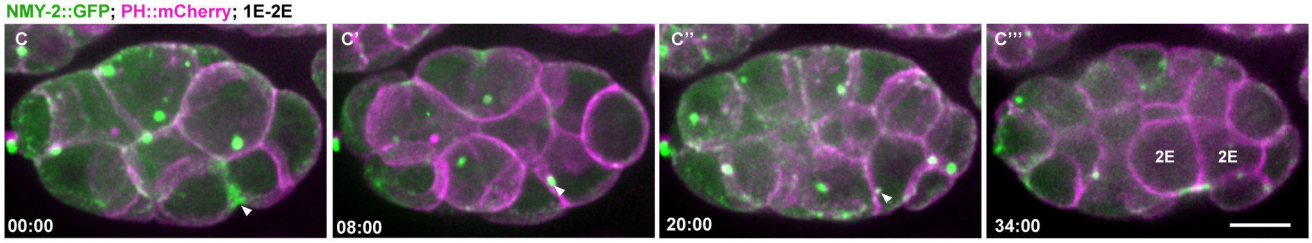

D

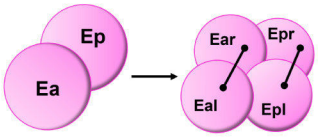

AIR-2::GFP; H2B::mCherry; PH::mCherry; 2E-4E

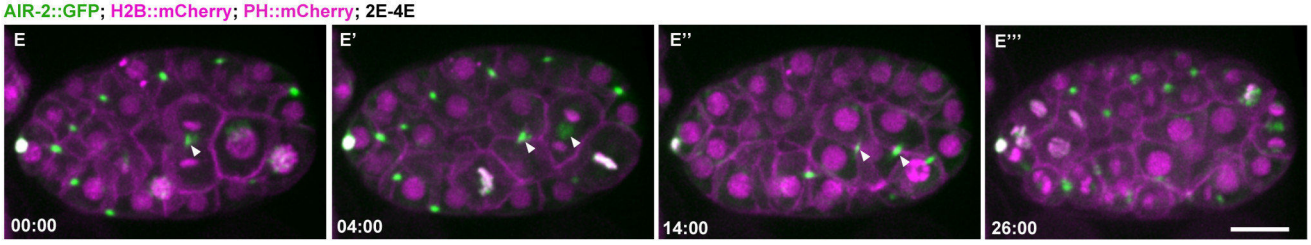

NMY-2::GFP; PH::mCherry; 2E-4E

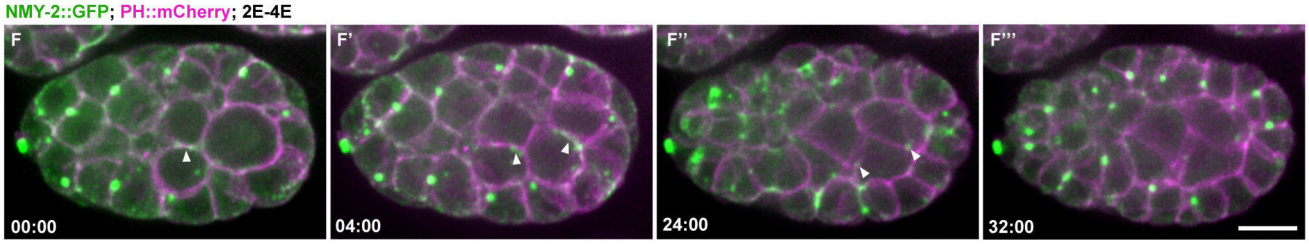

G

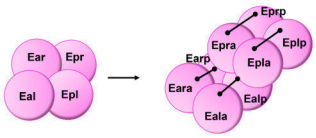

AIR-2::GFP; H2B::mCherry; PH::mCherry; 4E-8E

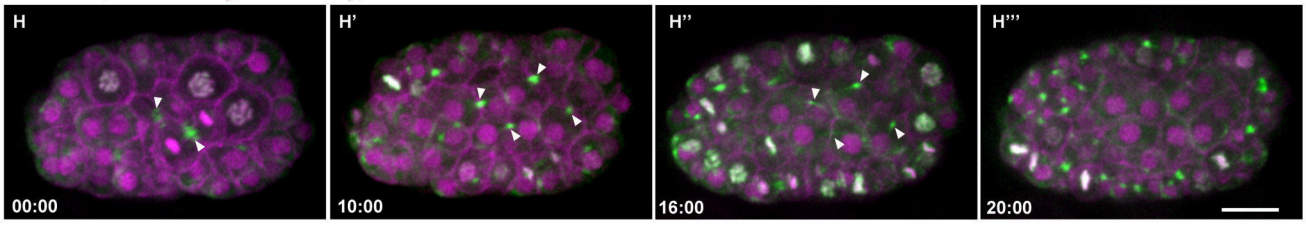

NMY-2::GFP; PH::mCherry; 4E-8E

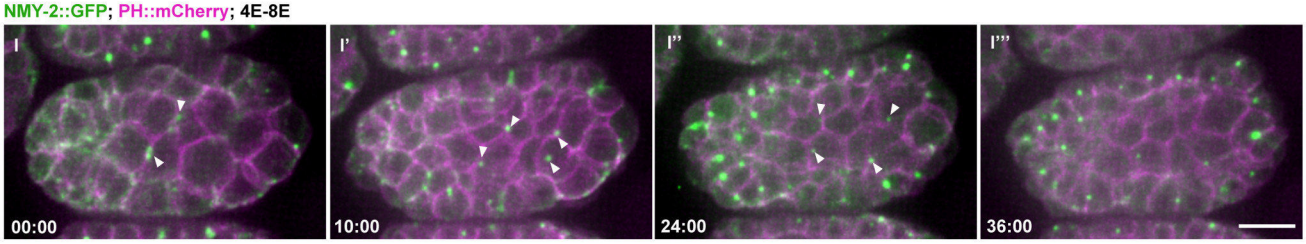

Supplement Figure 4

A

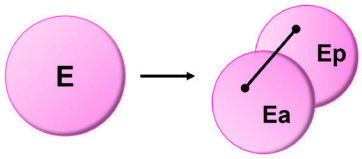

HMP-1::GFP; TBB-1::mCherry; 1E-2E

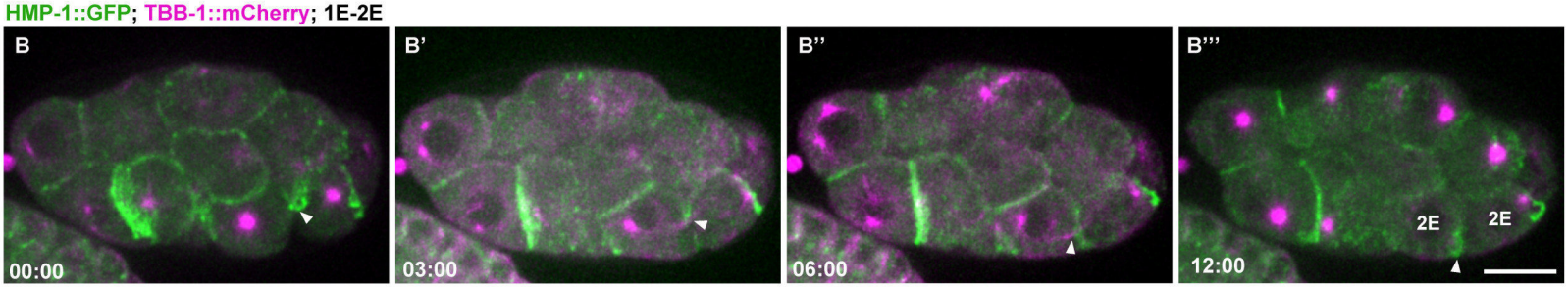

C

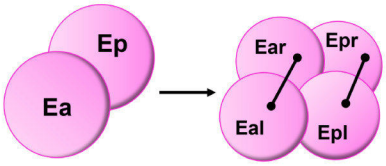

HMP-1::GFP; TBB-1::mCherry; 2E-4E

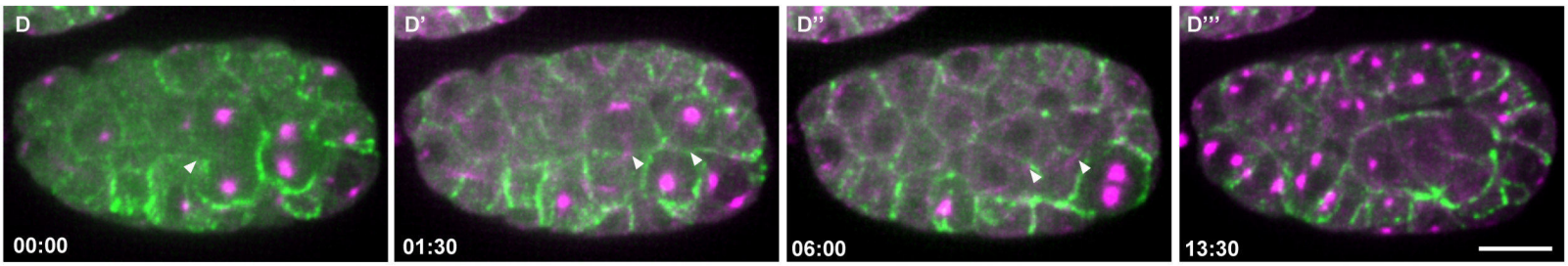

E

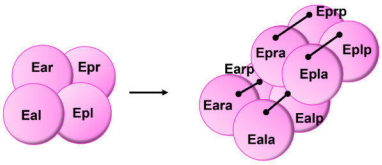

HMP-1::GFP; TBB-1::mCherry; 4E-8E

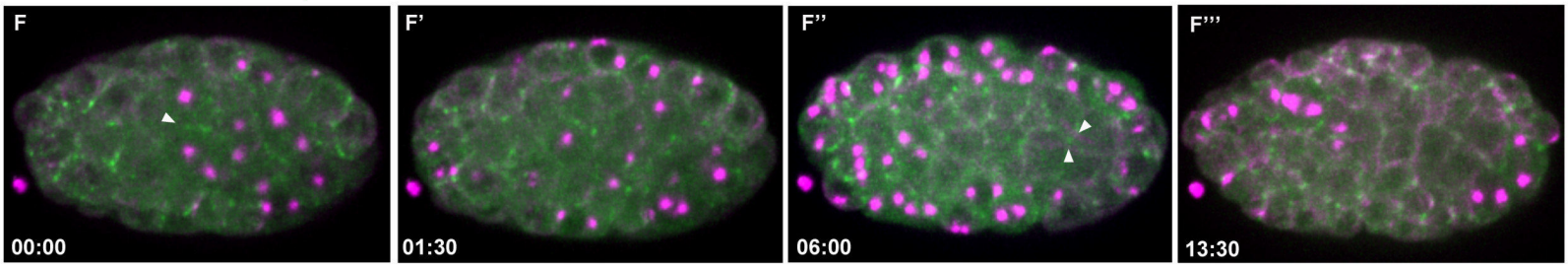

Supplement Figure 5

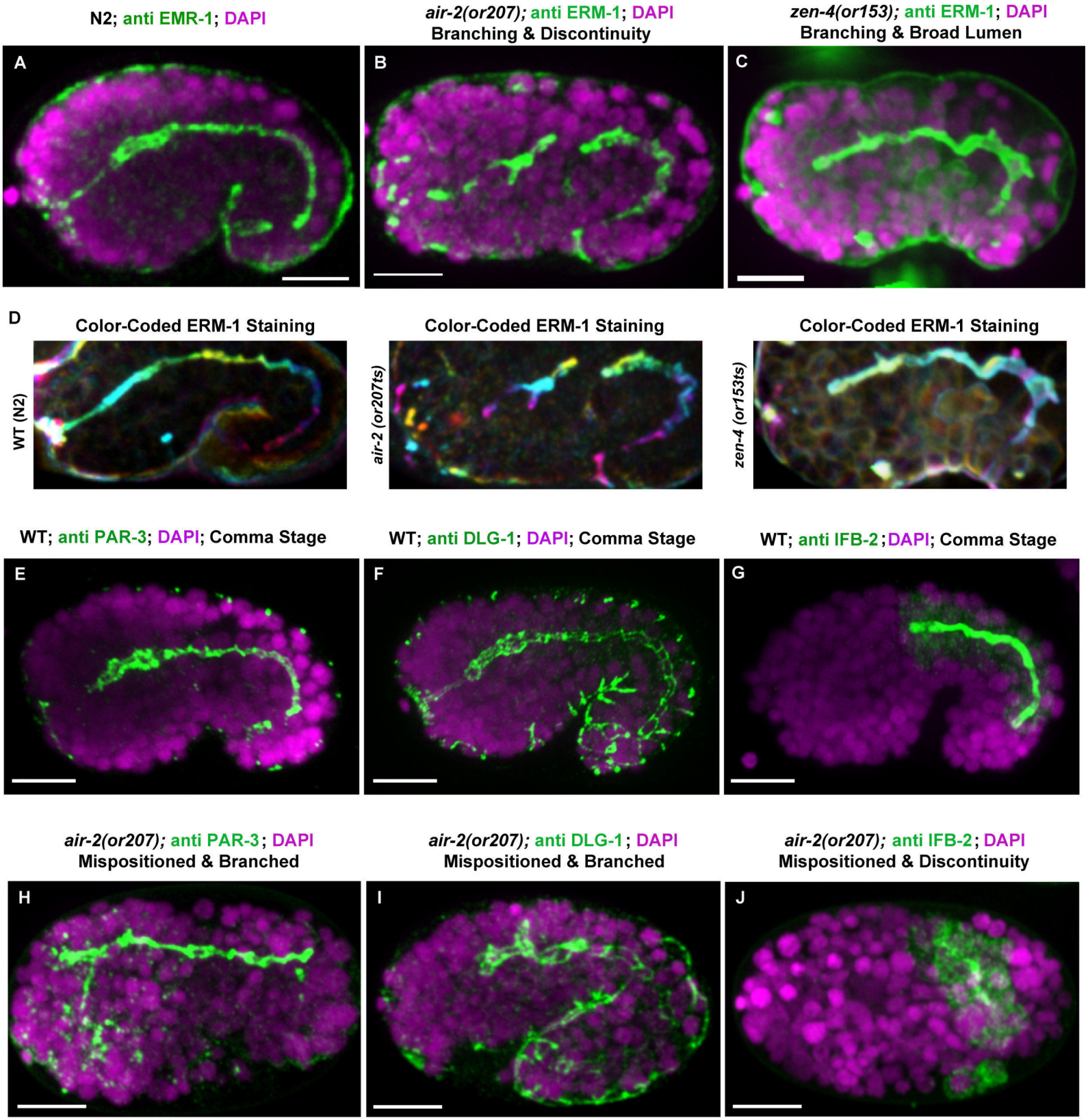

Supplement Figure 6

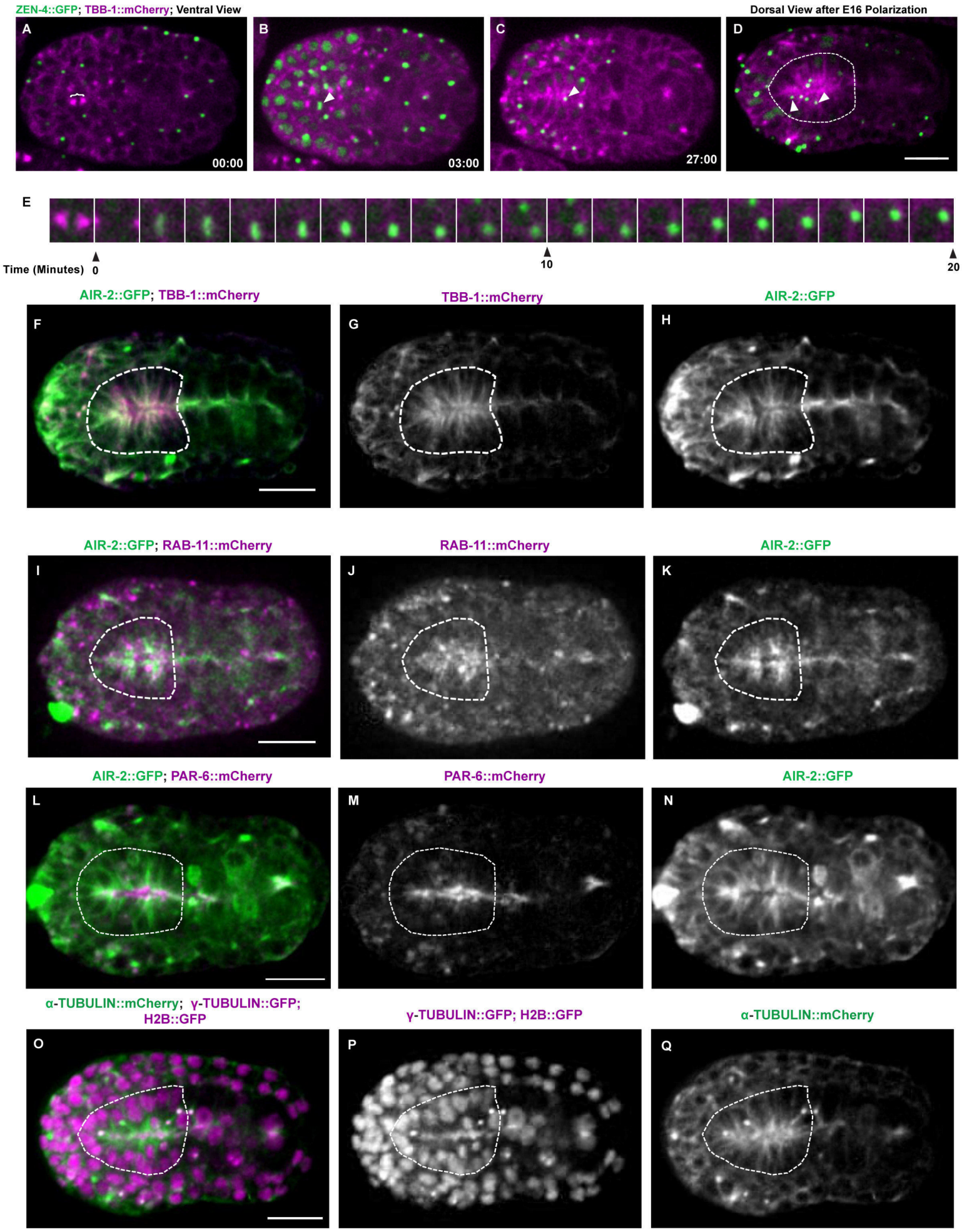
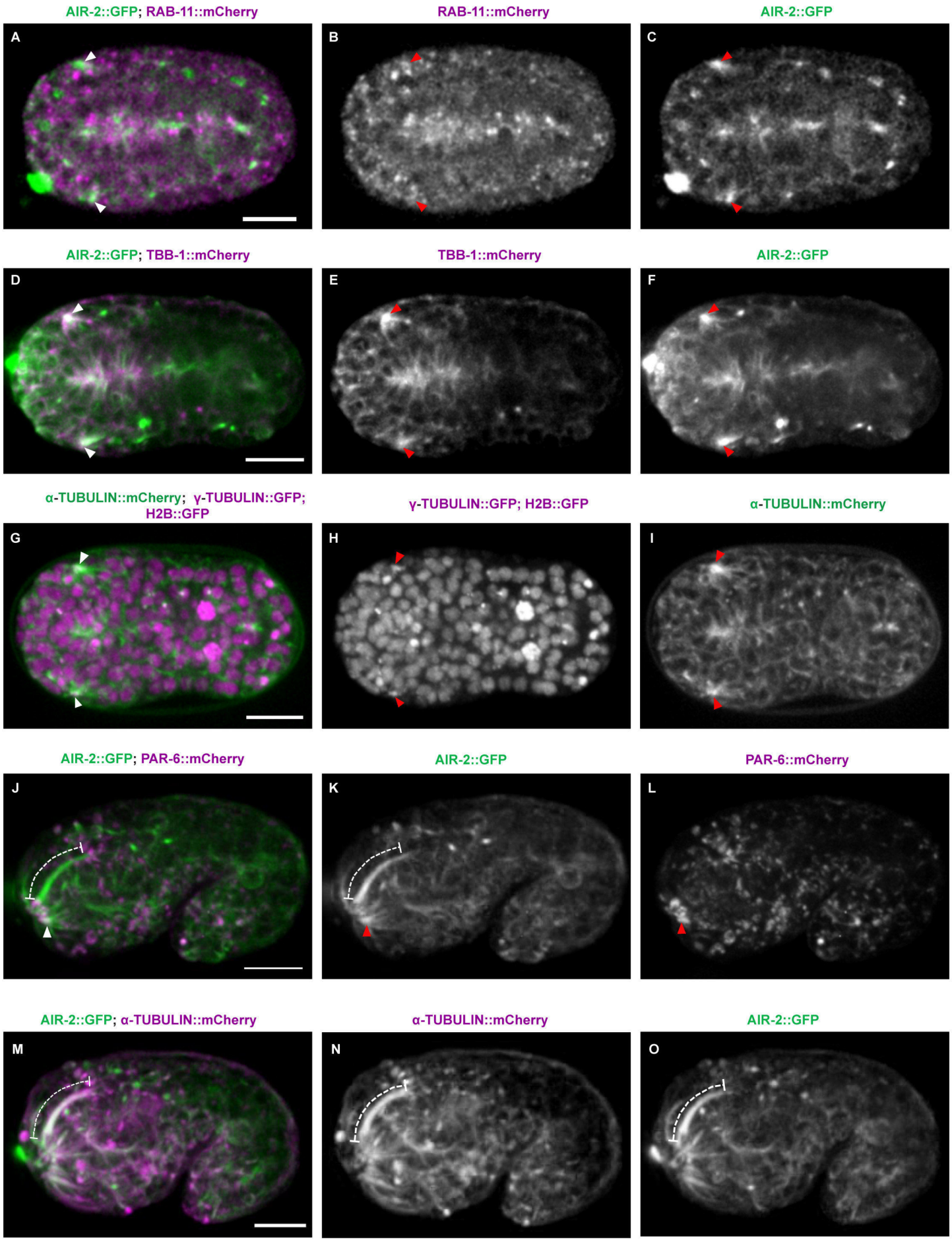
Supplement Figure 7